AD-A175 380 THEORETICAL RESEARCH INTO SOLID STATE DEVICES SUITABLE 1/1
FOR SUBMILLIMETRE OPERATION(U) CAMBRIDGE UNIV (ENGLAND)
DEPT OF PHYSICS J C INKSON 01 NOV 86 R/D-4442-EE-01
UNCLASSIFIED DAJA45-84-C-0048 F/G 20/2 NL

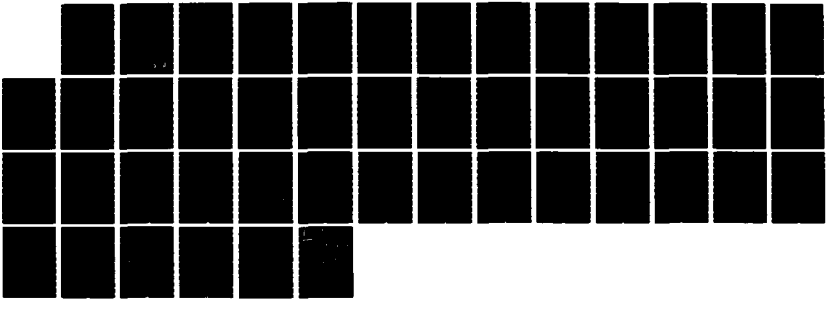

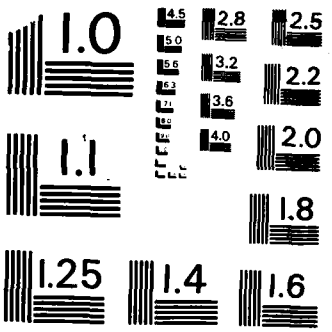

(12)

AD

THEORETICAL RESEARCH INTO SOLID STATE DEVICES SUITABLE FOR SUBMILLIMETRE OPERATION

Final Technical Report

by

J C Inkson

November 1986

United States Army

EUROPEAN RESEARCH OFFICE OF THE US ARMY

London England

CONTRACT NUMBER DAJ A45-84-C-0048

Contracting Office Dennis P Foley

UNCLASSIFIED
SECURITY CLASSIFICATION OF THIS PAGE

REPORT DOCUMENTATION PAGE

Form Approved
OMB No 0704-0188
Exp Date Jun 30, 1986

1a REPORT SECURITY CLASSIFICATION Unclassified	1b. RESTRICTIVE MARKINGS
2a. SECURITY CLASSIFICATION AUTHORITY	3. DISTRIBUTION/AVAILABILITY OF REPORT Approved for Public Release; distribution unlimited
2b. DECLASSIFICATION/DOWNGRADING SCHEDULE	
4 PERFORMING ORGANIZATION REPORT NUMBER(S)	5. MONITORING ORGANIZATION REPORT NUMBER(S) R&D 4442-EE-01
6a. NAME OF PERFORMING ORGANIZATION Dept of Physics University of Cambridge 6b OFFICE SYMBOL (If applicable)	7a. NAME OF MONITORING ORGANIZATION USARDSG-UK LONDON
6c. ADDRESS (City, State, and ZIP Code) University of Cambridge Old Schools Cambridge	7b. ADDRESS (City, State, and ZIP Code) Box 65 FPO NY 09510-1500
8a. NAME OF FUNDING/SPONSORING ORGANIZATION USARDSG(UK) ARO-E 8b OFFICE SYMBOL (If applicable) AMXSN-UK-RI	9 PROCUREMENT INSTRUMENT IDENTIFICATION NUMBER DAJA 45-84-C-0048
8c. ADDRESS (City, State, and ZIP Code) Box 65 FPO NY 09510-1500	10. SOURCE OF FUNDING NUMBERS PROGRAM ELEMENT NO. 61102A; PROJECT NO 1L161102BH57; TASK NO 03; WORK UNIT ACCESSION NO

11. TITLE (Include Security Classification)
(U)Theoretical Research into Solid State Devices Suitable for Submillimetre Operation

12. PERSONAL AUTHOR(S)
Inkson, John Christopher

13a TYPE OF REPORT	13b TIME COVERED	14 DATE OF REPORT (Year, Month, Day)	15. PAGE COUNT
Final	FROM 84.10.1 TO 86.9.30	86.11.1	41

16. SUPPLEMENTARY NOTATION
-

17. COSATI CODES		
FIELD	GROUP	SUB-GROUP
09	03	

18 SUBJECT TERMS (Continue on reverse if necessary and identify by block number)
Semiconductors, Devices, Heterojunctions, Superlattices, Quantum Wells, Interfaces, Submicron Structures, Tunnelling, Plasmons, GaAlAs alloys, Electron Transport

19 ABSTRACT (Continue on reverse if necessary and identify by block number)

The development of novel devices using submicron technologies is dependent upon a detailed understanding of the electronic properties at a quantum mechanical level. This report describes two related investigations into electron states and plasmons in heterojunction based quasi two dimensional systems formed from alternating layers of semiconductor material. It is found that the electron dynamics are no longer described by effective mass theory. Intervalley scattering, the excitation of localised states at the interfaces and the details of the electronic bandstructure are all important. Results are presented for electron scattering in the GaAs-GaAlAs system and resonant tunnelling through multiple barriers investigated. The plasmon modes are calculated by a new method which includes well widths, subband structure and multiple layers. This method allows the electron electron interaction in such a system to be calculated directly.

The consequences of this program for submicron device design are described and further work suggested.

20 DISTRIBUTION/AVAILABILITY OF ABSTRACT	21 ABSTRACT SECURITY CLASSIFICATION
☒ UNCLASSIFIED/UNLIMITED ☒ SAME AS RPT ☒ DTIC USERS	UNCLASSIFIED

22a NAME OF RESPONSIBLE INDIVIDUAL	22b TELEPHONE (Include Area Code)	22c OFFICE SYMBOL
Dr. James W. Gault	01-409 4423	AMXSN-UK-RI

DD FORM 1473, 84 MAR 83 APR edition may be used until exhausted
All other editions are obsolete

SECURITY CLASSIFICATION OF THIS PAGE
UNCLASSIFIED

CONTENTS

ABSTRACT

The development of novel devices using submicron technologies is dependent upon a detailed understanding of the electronic properties at a quantum mechanical level. This report describes two related investigations into electron states and plasmons in heterojunction based quasi two dimensional systems formed from alternating layers of semiconductor material. It is found that the electron dynamics are no longer described by effective mass theory. Intervalley scattering, the excitation of localised states at the interfaces and the details of the electronic bandstructure are all important. Results are presented for electron scattering in the GaAs-GaAlAs system and resonant tunnelling through multiple barriers investigated. The plasmon modes are calculated by a new method which includes well widths, subband structure and multiple layers. This method allows the electron electron interaction in such a system to be calculated directly.

The consequences of this program for submicron device design are described and further work suggested.

KEYWORDS INCLUDE:

1 Semiconductors,
2 Devices,
3 Heterojunctions,
4 Superlattices,
5 Quantum Wells
6 Interfaces
7 Submicron Structures
8 Tunnelling
9 Plasmons
10 GaAlAs Alloys
11 Electron Transport
12 Bandstructures

I INTRODUCTION

Any understanding of the operation of a semiconductor device must be based upon a realistic microscopic model. The dimensions and growth techniques used since the 1960's have meant that a quasi classical treatment based upon effective mass theory and the Boltzmann equation have, with few exceptions, proved sufficient. The advent of heterojunction based submicron structure fabricated by MBE MOCVD or other related technology, however, has produced a whole range of devices both realised and proposed (1) whose atomic scale negates the basic assumptions of semi classical device design and quantum effects become predominant (1,2). In spite of this, standard theory has continued to be used for both device design and interpretation of experimental data with some success (1,2).

The purpose of the project was twofold:

(A) to develop a basis for device design from a microscopic approach so that quantum transport could be considered in a realistic manner.

(B) To look at quantum effects, in particular the plasmon modes in single and multiple quantum well systems.

The overall framework was the development of millimetre wave sources, such as the orotron (free electron laser), in which fast electrons could interact with the space charge produced by plasmon excitation to form a distributed source free from the normal transit time-size limitations (3).

Because these two areas are disparate, in that the techniques required are quite different, we have split the technical report into two sections, A and B. These describe the work in the electron states and plasmons respectively. They can largely be read independently.

The summary, Section III, relates the two areas together and draws some conclusions and suggestions for further work.

II TECHNICAL REPORT

A ELECTRON STATES

A1 Introduction

When a device becomes so small as to be of atomic dimensions one cannot expect either the effective mass approximation or the Boltzmann transport equation to hold, but in the absence of anything better both have been used extensively for the whole range of heterojunction based submicron device studies (1,2). In the last two years we have pursued a vigorous programme of work designed to put the calculations of electron states and transport porperties on a firm microscopic footing (4,5,6,7,8).

The basis of our calculations has been a careful study of the scattering of electron states from a single heterojunction interface (4). We have used an empirical pseudopotential description of the two semiconducting materials, which gives good electron states and bandstructures, and then used the resulting states in a matching routine which produces all of the possible excitations at the interface as well as the reflection and transmission coefficients of the carriers as a function of energy and internal momentum (4,5,8). The related tight binding methods (11,12) suffer from an inherent limitation as to accuracy of band gaps and effective mass.

This approach, although not as direct as say a supercell calculation for obtaining electron states in a quantum well (9,10), is extremely flexible. We have used it to obtain not only quantum well states (6,8) but also barrier tunnelling probabilities (7), resonant tunelling through double barriers (7) and we are now in the position to calculate the effect of any combination of wells, barrier thicknesses and alloy compositions (7). In all of these calculations the effect of alloy concentration, higher minima, non parabolicity and the relationship to effective mass theory have all been considered. What we have now is probably the most flexible and powerful technique for considering electron states in heterojunction based systems.

A2 The Method

Consider first of all the simplest situation conceivable: a single GaAs/AlGaAs junction, and let the electron, in state $|k\rangle$, be incident normal to the interface from the GaAs side. In the EMT representation we have an incident wave, the reflected wave and *one* tunnelling (or evanescent) state of wavevector $-i\gamma$ [fig 1(a)]. We may express this mathematically as

$$e^{ik.R} + Re^{-ik.R} = Te^{-\gamma.R} \qquad 1$$

where R and T are the reflection and transmission coefficients, respectively. It is illuminating to look at the problem in a different way. By considering real energies below the bottom of the conduction minima, we obtain complex values of $k_\perp$ (13,14). Consider the EMT approximation of a semiconductor bandstructure (fig 1b). Here, the full lines represent the real bandstructure (assumed to be parabolic) and the

broken lines represent the complex bandstructure. Hence, at any particular energy below the top of the well, the electron can connect or excite only one evanescent state. The other evanescent state ($+iy$) corresponds to a wave growing exponentially away from the interface, which is unphysical in this particular case.

Above the well the evanescent state becomes the transmitted state carrying the electron current above the barrier. In a real semiconducter there are many possible states at a given energy with complex wavevectors, which can be excited at the interface by the incident electron state, coming off the higher conduction bands in the system. These may all contribute to the reflection and transmission process at the interfaces.

The basis of the calculation is, therefore, the matching, for a given energy and momentum parallel to the interface, of the set of eigenstates of the two semiconductors for a given incoming electron state. The eigenstates include not only the Bloch states of the bulk materials but also the evanescent states available through the removal of the translational symmetry perpendicular to the surface. The methods used to calculate the bulk eigenstates have been previously described in detail elsewhere (15). Basically a layer method (16) is used, employing empirical pseudopotentials (17,18). A virtual-crystal approximation is used for the alloy system and, in order to avoid lattice mismatch, the GaAs interatomic distance always taken. This will not introduce any appreciable error since the maximum lattice mismatch is always < 0.4 %.

Figures (2a) and (2b) show the $k_{\parallel} = 0$ bandstructure for a (100)GaAs-AlAs interface as an example of the heterostructure calculations. The complex bands N13,14) derive not only from the Γ minimum but also from all of the higher real bands. One should note for later reference that the complex bands are <u>highly</u> non-parabolic. For instance, the band originating from the bottom of the AlAs conduction band state gives a complex wavevector that is almost independent of energy over an energy range of ~1.2eV, i.e. covering a good proportion of the bandgap.

Given the eigenstates at a particular energy and parallel momentum, one sets up the matching condition at the interfaces which may be expressed schematically as:

$$|\text{incident}\rangle + \Sigma R_i|(\text{reflected})\rangle_i + \Sigma a_i|(\text{evanescent:1})\rangle_j \quad \langle\langle = \rangle\rangle \quad \Sigma T_l|(\text{transmitted})\rangle_l + \Sigma b_m|(\text{evanescent:2})\rangle_m \qquad 2$$

where the R_i, T_l are the reflection and transmission coefficients for the Bloch states while the a_j, b_m are those of the evanescent waves excited in the two media at the interface. The magnitude of a_j, b_m represent how strongly the incident Bloch wave is coupling to the available evanescent states. (Some of the a_j, b_m must be set to zero since they represent waves which grow exponentially away from the interface and are therefore unphysical.)

Equation (2) is set up as a series of simultaneous linear equations expressing continuity of the wavefunction and its derivative for each of the lattice vectors of the interface reciprocal lattice. The matrix equation represented by this set is then solved to give the coefficients R, T, a, b. Obviously, the number of surface reciprocal lattice vectors

(equivalent to the number of states involved) needs to be restricted to a finite number at some point. We have taken up to 13 surface reciprocal lattice vectors but find that 7 gives less than 5% changes in the results between the two cases.

There are a number of checks that can be made on the calculation of which the most important is the current conservation across the boundary. In all cases we have obtained current conservation within 1×10^{-4}%. Another useful check is the symmetry of the wavefunction. At $k_{\parallel} = 0$ the bands in figures (2a) and (2b) have differing symmetries with regard to the 2D interface lattice. This means that some will not take part in the scattering process. We did not perform a symmetry separation of the matching matrix equation on the basis that for $k_{\parallel} \neq 0$ the symmetry is broken down anyway, but even so the coefficients for the 'forbidden' symmetry states were down by four orders of magnitude relative to the allowed states. We thus have confidence in the results of our program.

For a multiple interface, as in a quantum well or multiple barrier system, one can extend the analysis by allowing for more than one incident state. If we consider 2N eigenstates in each region (corresponding to N propagating or decaying in either direction) then the situation is as follows (fig 3).

The calculation proceeds by first selecting a state, with wavevector $k = (k_{\parallel}, k_{\perp})$ and energy E, from the (calculated) bulk band structure. The selected state is then designated as the incident wave and may be viewed as propagating towards the first interface, of an m-interface device, with a group velocity determined from the curvature of the band structure. Upon reaching the first interface it will excite $3N$ evanescent and (possible) continuum states. N of the states will exist in region 1 and consist of waves decaying or propagating to the left. The second region accommodates the remaining $2N$ states which comprise waves propagating and decaying to the left and the right (fig 3). Thus for a structure of m interfaces a total of $2Nm$ states will be excited by the incident wave. The case of N=1, which corresponds to the effective-mass approximation, has been considered previously by Tsu and Esaki (19).

At each interface the wavefunction and its derivative are matched smoothly. This gives a matrix equation relating the amplitudes of the coefficients of the wavefunction on one side of the junction to those of the other side. We write the wavefunction in the nth region as:

$$\Psi^n = \sum_{i=1}^{2N} a_i^n \psi_i^n \qquad 3$$

with $i < n < m$ and ψ_i^n the known bulk eigenstates.

Constructing a matrix equation relating the set of coefficients $\left[a_i^n\right]$ on the nth side of the junction to those on the $(n + 1)$th side $\left[a_i^{n+1}\right]$ gives

$$\begin{bmatrix} \psi_1^n & \cdots & \psi_{2N}^n \\ \vdots & & \vdots \\ \psi_1^n & \cdots & \psi_{2N}^n \end{bmatrix} \begin{bmatrix} a_1^n \\ \vdots \\ a_{2N}^n \end{bmatrix}$$

$$= \begin{bmatrix} \psi_1^{n+1} & \cdots & \psi_{2N}^{n+1} \\ \vdots & & \vdots \\ \psi_1^{n+1} & \cdots & \psi_{2N}^{n+1} \end{bmatrix} \begin{bmatrix} a_1^{n+1} \\ \vdots \\ a_{2N}^{n+1} \end{bmatrix} \quad 4$$

$$\begin{bmatrix} a_1^n \\ \vdots \\ a_{2N}^n \end{bmatrix} = S_{n,n+1} \begin{bmatrix} a_1^{n+1} \\ \vdots \\ a_{2N}^{n+1} \end{bmatrix} \quad 5$$

Here $S_{n,n+1}$, the S-matrix for the nth interface, is a function of the barrier height, position of the junction and electron energy. For adjacent junctions we similarly calculate $S_{n-1,n}$ and $S_{n+1,n+2}$. We may then relate the incident and output states by the equation:

$$\begin{bmatrix} a' \\ \vdots \\ a_{2N} \end{bmatrix} = (S_{12}S_{23}S_{34} \cdots S_{m-1,m}) \begin{bmatrix} a^{n+1} \\ \vdots \\ a_{2N}^{n+1} \end{bmatrix} \quad 6$$

where the development of the states between junctions is found by application of the Bloch relation for the bulk states.

Thus at each junction we have to calculate an S-matrix which relates the $2N$ coefficients on each side of the junction to each other. The total scattering matrix S, which relates the set of coefficients (a_i^1) of the incident state to the set (a_1^m) of the output state is given by:

$$S = S_{12}S_{23}S_{34} \cdots S_{m-1,m}. \quad 7$$

The power of the S-matrix approach is the way in which it reduces the original problem from the diagonalisation of a $2Nm \times 2Nm$ matrix to the calculation of m $2N \times 2N$ matrices.

To obtain physical solutions for a finite structure we also need to set the coefficients of the waves which grow exponentially away from the 1st and mth interfaces equal to zero. In the case of a superlattice, periodicity makes all of the matrices equivalent (apart from a phase factor) and the problem reduces to the calculation of a single $2N \times 2N$ complex matrix.

Having obtained the coefficients $\left[a_i^1\right]$ and $\left[a_i^m\right]$ we need to calculate some quantity of interest. One such quantity is the current transmission

probability (T) through the device (20). This may be defined by:

$$T = \frac{\Sigma_{j=1}^{N} \left|a_j^m\right|^2 \mathrm{Re}\left[\psi^*_{k_{1j}^m}\left[-i(\delta/\delta z)\psi_{k_{1j}^m}\right]\right]}{\mathrm{Re}\left[\psi^*_{k_{1i}^1}\left[-i(\delta/\delta z)\psi_{k_{1i}^1}\right]\right]} \qquad 8$$

where the subscript i refers to the state chosen as the incident wave. For an incident energy above the GaAs X_1 minima, part of the transmitted flux will be carried by the X_1 continuum state of the GaAs. It has been shown by Marsh (20) that it is possible to subdivide the transmitted flux into the contributions from the Γ_1 and X_1 states. This allows one to define further current transmission coefficients T_x and T_r, the sum of which gives T. Conversely, the reflected flux can similarly be divided, giving reflection coefficients R_x and R_r.

A3 Results

The first set of results refer to the single interface. We have calculated the reflection and transmission coefficients for a whole range of alloy compositions for the GaAs-GaAlAs system for the three surfaces (1,1,1) (1,1,0) and (1,0,0) (4,5,6). We will concentrate only upon the (1,0,0) results. The bandstructures of the two media are shown in figures (2a) and (2b) and one sees that for a state in the conduction band the states of prime interest are the Γ and X states. There are two X states of importance which we have labelled X_1 and X_3. These X states are essentially identical below the X minimum being the two states which come off the $\pm k_{min}$ points in the upper band but above the minimum the k values split, one going towards the zone centre (X_1) and the other to the zone edge and then on up through the X_3 point into the higher Δ_1 band (X_3). We obtain the band mismatch simply from the juxtoposition of the two calculated bandstructures. In essence this amounts to ignoring any charge transfer effects. For the GaAlAs system this is a good approximation (9). This gives results (fig 4) within the experimental range but if necessary the mismatch can be altered by simply incorporating a constant potential to rigidly move the bands relative to one another.

Figures (5) and (6) show the excitation levels of states produced by an electron in a Γ state incident in the GaAs on an alloy of GaAs-AlAs as a function of incident energy. (All of the other states involved are four orders of magnitude down in amplitude.) The points to note are that

i The higher X states are <u>not</u> negligible and a very strong resonance occurs in their excitation around the X minimum energy in the GaAs.

ii The transmission and reflection coefficients for the Γ states have a magnitude which is not too different from that which may be expected in the effective mass limit.

iii As the energy of the incident states increases some of the states change from evanescent to propagating states and the amplitudes are then related to the transmission probabilities, ie figures (5) and (6) show strong intervalley transfer in both reflection

and transmission.

The application of these scattering amplitudes to quantum wells may be performed in two ways. Firstly, consider an electron of energy E incident on the interface in the Γ_1 minimum of the GaAs with wavevector $(k_\perp, k_\parallel)$. Provided the energy is below that of any higher minima in either material then electrons will simply be scattered back into the $(-k_\perp, k_\parallel)$ state in the Γ_1 minima. (There will also be excitation of the evanescent states but this is the only propagating solution present.) It follows that we can express the reflection coefficient as:

$$R = \exp(i\phi(E,k)) \qquad 9$$

where ϕ is the phase shift of the incident electron upon reflection at the heterojunction interface and wil be a function of the energy and momentum. The evanescent waves are localised at the interface, so provided one is interested in the 'long distance' behaviour they may be ignored, apart from their implicit effect on the values of ϕ. (This is entirely analogous to the standard problem of reflection from discontinuities in waveguide systems.) Fig 7 shows a typical curve for ϕ for an alloy concentration of x = 0.25.

Consider now the distance scales involved. In a typical GaAs–$Ga_{1-x}Al_xAs$ quantum well we are concerned with widths of the order of 50 Å and above. However, the evanescent states on the GaAs side are confined, typically, to within ~10 Å of the interface since they originate from the L, X or higher minima. Thus, if we wish to calculate the eigenstates of quantum wells we may do so on the basis of a standard single-minimum model *provided* we take account of the real reflection phase rather than the simplistic effective-mass value.

Consider for instance a square quantum well. Remembering that the equations are linear the wavefunction at the centre of the well is given by the combination of incident and reflected states, so for a well of width 2L and centre at -L we have:

$$\psi_E(-L) = (\text{constant}/\sqrt{2})(|k_\perp, k|, -L\rangle + e^{i\phi}|-k_\perp, k_\parallel, -L\rangle) \qquad 10$$

provided, as we have said, that the well width is much larger than the evanescent decay length. For eigenstates of the well we require either:

$$\psi(-L) \neq 0 \; ; \; \left.\frac{\delta\psi(z)}{\delta z}\right|_{-L} = 0 \qquad \text{symmetric state} \qquad 11a$$

or

$$\psi(-L) = 0 \; ; \; \left.\frac{\delta\psi(z)}{\delta z}\right|_{-L} \neq 0 \qquad \text{antisymmetric state} \qquad 11b$$

Taking only the envelope part of the wavefunction (the cell periodic part for practical wells will produce only relatively small shifts in the answer) this gives

$$2k_\perp L + \phi(E,k_\perp) = (2n+1)\pi \qquad \text{symmetric state} \qquad 12a$$

or

$$2k_1L + \phi(E,k_1) = 2n\pi \qquad \text{antisymmetric state} \qquad \underline{12b}$$

which can be compared directly with the effective-mass result by using the effective-mass values for ϕ. This can obviously be extended for both space-charge-dominated (eg heavily doped superlattices) and the case where more than one propagating wave is produced. The essence of the approximation is the existence of the two scale lengths - one for the evanescent waves which are localised at the interface and one for the quantum well width. The effect of the interface is only felt by the reflection coefficient ϕ. Obviously if we consider very small well widths ($\leq$ 30 Å) we will have to be more careful.

This formalism has the advantage that we only have to work out the phase shift once for any given alloy concentration. A graphical solution of (12) is shown in fig (7). This figure also illustrates the effective mass phase shifts using two different boundary conditions. The first, EMT(1), involves the matching of wavefunction and derivative at the interface

$$\left.\frac{\delta\psi^{GaAs}(z)}{\delta z}\right|_{z=0} = \left.\frac{\delta\psi^{AlGaAs}(z)}{\delta z}\right|_{z=0} \qquad \underline{13}$$

This has the problem that in order to conserve current it is necessary to renormalize the wavefunction. The second method [EMT(2)] is to equate the wavefunction and its derivative divided by the appropriate effective mass

$$\left.\frac{1}{m_1^*}\frac{\delta\psi^{GaAs}(z)}{\delta z}\right|_{z=0} = \left.\frac{1}{m_2^*}\frac{\delta\psi^{AlGaAs}(z)}{\delta z}\right|_{z=0} \qquad \underline{14}$$

This allows current conservation to be maintained without the renormalization of the wavefunction. The difference is the intersect in figure (7) gives an estimate of the errors involved typically $\leq$ 10 % for EMT2. We would expect this deviation from EMT to become more pronounced for well widths below 50 Å. In this instance, a significant coupling between the evanescent states at the quantum well interfaces will start to occur.

A purely numerical evaluation of the quantum well states is possible by using the multiple interface scattering matrix techniques by looking at the reflectivity of an "incident" growing exponential on the well. My colleague A C Marsh has recently been working on this approach (21) and figure (8) shows the results for a range of quantum well widths. It is noticeable that the errors in effective mass theory do grow as we would expect for narrow wells but the lowest state remains remarkably accurate and, provided nonparabolicity is taken into account, the higher bands are quite well described (22). However, this does not imply that the EMT approximation is in any way valid, since the associated *eigenfunctions* are liable to be different from their true counterparts (23). This will, for instance, lead to reduced electron-phonon or electron- plasmon scattering, since the contributions of the wavefunction from the X_1 and X_3 will have been neglected in the matrix elements.

To illustrate the *S*-matrix technique we have applied it to the relatively simple example of a (100) double barrier (m=2) and modelled each bulk semiconductor with 13 surface reciprocal lattice vectors (N=13). This particular geometry is especially interesting in the case of a device based upon GaAs and AlAs. In this instance the positions of the X minima form two potential wells for the electrons, fig (9).

Firstly, consider what would be expected from an effective mass description. With infinite confining barriers we have an isolated well and a series of bound states. If the confining barriers are of a finite width, the electron in the well has a finite probability of tunnelling through the confining barriers and so the bound states would become resonances in the current transmission coefficient. The widths of these transmission resonances would broaden out as the widths of the confining barriers were reduced, reflecting the increasing probability of tunnelling through the confining layers. Since this depends upon general quantum mechanical principals we would not expect any qualitative change in the picture of a series of resonances in the transmitted electron current. Using the more sophisticated pseudopotential description, we would also expect elastic intervalley transfer between the Γ and X valleys to be significant if the energy of the incident electron is greater than ~ 0.3 eV. This effect would be especially important in wide barriers with compositions greater than ~ 0.45 where the magnitude of the current associated with the propagating X state may be many orders of magnitude higher than that of the Γ tunnelling current (20). Secondly, there may also be resonances in the transmission coefficient associated with the interaction of the electron with the X valleys. Such effects were clearly visible in the calculations of a single interface (fig 6), (4,5,6). Thirdly, given the geometry considered, the X_1 states of the system form two wells, which are separated by a barrier of GaAs, and so effects associated with the interaction of these X-like wells may also be seen, possibly as structure in the transmission coefficient.

We have calculated the current transmission coefficient (T) as a function of incident electron energy for a series of well widths from ~ 11 to ~ 71 Å. Two typical results are shown in figures (10) and (11). We have purposely kept the widths of the confining barriers constant to concentrate on the properties of the central GaAs region. The figures also show the equivalent EMT result, using the effective masses and barrier heights calculated from the pseudopotential model. The most prominent features of all the results are the resonances in the transmission probability. These relate closely to the expected energies of the middle well resonant states. Although these are also seen in the effective mass results, there are considerable quantitative differences between the two approaches. Note that the influence of the X-valleys can also be seen as two resonances in the transmission coefficient at E^X_{T1} and E^X_{T2}. These were also seen in the calculation of a single tunnel junction (20). The positions of the "X" resonances remain fixed at all well widths considered, confirming their origin as the influence of the X_1 GaAs and X_1 AlAs valleys.

In order to assimilate the data more readily we have plotted the positions of the numerical and effective mass (17) resonance positions as a function of energy and central GaAs layer width, (fig 12). Only the lowest (n=1) resonance is reasonably well represented by the effective

mass model, a maximum deviation of ~ 10 % between the EMT and numerical results being apparent. The higher (n=2 and n=3) energy resonances show a larger (~ 30 %) discrepancy with those predicted by EMT.

Note that the position of some resonances, with energies close to the top of the well, are not predicted by the effective mass model.

It is interesting to explore further the nature of the resonances at $E_{\Gamma 1}^{X}$ and $E_{\Gamma 2}^{X}$ by calculating T_X and T_Γ. These are plotted in figure (13) for a well width of ~ 11 Å. Here, the two resonances are clearly visible. The first of these at $E_{\Gamma 1}^{X}$ is associated with a corresponding resonance in the coefficients of the wavefunction in the AlAs region, whilst the second is due to the sudden increase in the X reflected current as the X_1 GaAs minimum is approached. This is exactly what was found in the case of a single tunnel junction (21). The diagram also illustrates that at $E_{\Gamma 2}^{X}$ the X transmitted flux at 0.4 eV is higher than the Γ current. Thus in this particular energy range more current is being transported by the X GaAs state than by the Γ state. An interesting aspect of figure (13) is that the transmission coefficient (T) is not equal to unity at the resonance energy. At the Γ resonance ~ 20 % of the transmitted flux is reflected back into the GaAs X_3 valley, whereas the effective mass model would predict unity transmission.

These results in particular emphasise the power of the method. The transmitted current calculations are closely related to the I-V characteristics one might expect in a device (19,24) (we are at present developing the formalism to take into account directly the effect of an electric field). This means that we are close to a microscopic evolution of non periodic structures such as the CHIRP (25,26) and "Staircase" (27) devices, neither of which are amenable to supercell type calculations.

A4 Summary

The ability to evaluate the electron states on a microscopic basis has been shown to be possible for the quantum single and multiple well systems without the necessity of periodicity. This is of immense importance because practical devices will of necessity use the power of MBE and MOCVD fabrication techniques to produce a whole range of structures. Any method which is based upon periodicity therefore will have only limited application. The "dynamic" nature of our calculations should be stressed. Whereas the supercell type of calculation gives as a result the eigenstates and eigenenergies our method connects directly to the concepts of electron transport and flux. This is especially important in any attempt at device modelling.

Our results show that the effects of nonparabolicity, and the higher minima cannot be neglected in any discussion of electron transport in these systems.

B PLASMON MODES

B1 Introduction

The plasmon modes, due to the oscillation of electrons in a quantum well system, form a mechanism for either energy loss or energy gain depending upon the precise conditions prevailing in the device. That is they may be important in both normal electron transport and in active power generation devices. The interaction of electrons with the plasmon modes will depend upon the properties of these modes and, since we are working on a microscopic scale, it is important that any theory of the properties of the plasmons be compatible with the electron states of the system. In other words it is no use developing a microscopic theory for the electron states and then using a continuum model for the plasmons.

Over the last two years in parallel with our work on the electron states we have developed a microscopic theory for the plasmon modes (28,29) which

(a) is dependent upon the details of the electron states in the system, incorporating the possibility of both multiple subbands and varying numbers of wells. That is it avoids the common assumptions of simplified model systems (30,31,32,33).

(b) gives a realistic evaluation of the energies of all the possible modes.

(c) allows the calculation of the matrix elements necessary in any transport equations.

Recently there has been much interest in the theoretical calculation of the plasmon dispersion relationship of a superlattice (Bloss (30), Sarma and Quinn (31), Giuliani, Qin, and Quinn (32), and Tselis and Quinn (33)). Much of the work has approached this problem using expressions for the dielectric-response function in reciprocal space. The plasmons are then given by the frequencies for which the determinant of the infinite dielectric matrix goes to zero. In this pAper we take the alternative approach of calculating the inverse response function using a real-space formalism which gives the plasmon modes as its poles. The advantage of this technique is that the resulting expressions are in the form required to calculate interaction effects so that the contribution of the plasmon poles can be seen directly in, for example, the self-energy and inelastic processes.

It is important to realize that for many applications the knowledge of the plasmon poles themselves is insufficient. One must also have the screened interaction. This is given by the expression (34)

$$\int \epsilon(\underline{r},\underline{r}'',\omega)v(\underline{r}''-\underline{r}')d\underline{r}''$$

and so involves an accurate knowledge of the inverse response function and its spatial variation. This in turn requires that the model used for ϵ and hence ϵ^{-1} includes realistic eigenstates.

It is the screened interaction which gives information about the matrix elements whilst the use of real space techniques makes sure that the non periodic systems such as a single or even a small number of coupled wells can be treated within this formulation.

B2 Method

The dielectric response function in the random-phase approximation is

$$\epsilon(r,r',\omega) = \delta(\underline{r}-\underline{r}') - \int \nu(\underline{r}-\underline{r}'')\, P(\underline{r}'',\underline{r}',\omega)\mathrm{d}\underline{r}'' \qquad 15$$

where

$$P(\underline{r}'',\underline{r}',\omega) = \sum_{\underline{k},\underline{k}'} \frac{2\left[n_{\underline{k}} - n_{\underline{k}'}\right]}{E_{\underline{k}} - E_{\underline{k}'} - \hbar\omega - i\delta}\, \psi_{\underline{k}}(\underline{r}'')\psi^{*}_{\underline{k}'}(\underline{r}'')\psi^{*}_{\underline{k}}(\underline{r}')\psi_{\underline{k}'}(\underline{r}') \qquad 16$$

where all the symbols have their usual meanings.

To model the superlattice we take it to be a series of equally spaced quantum wells with centres separated by a distance a. Along the wells we assume that the motion is unrestricted whilst in the perpendicular direction we have localised quantum well wavefunctions forming a series of tight-binding-like subbands. The energies and number of these subbands are determined principally by the quantum well properties. In the usual notation we have for such a system

$$\psi^{(\alpha)}_{\underline{k}}(\underline{r}) = \frac{1}{N^{1/2}}\,\frac{1}{\Omega^{1/2}} \sum_{m} \exp\left[i\underline{k}_{\parallel}\cdot\underline{\rho}\right]\exp\left[ik_{\perp}ma\right]\phi^{(\alpha)}(x - ma) \qquad 17$$

where (α) is a sub-band index.

The states $\phi^{\alpha}(x)$ may be obtained either from a model calculation or through calculations such as those of Section A. In this calculation we take it that there are two sub-bands, the Fermi level being such that only the lower ($\alpha = L$) is occupied, and ignore level broadening due to tunnelling between the wells. The extension to more than two sub-bands is straightforward.

Using the translational invariance of the Hamiltonian parallel to the planes a little algebra shows that we can write the Fourier transform of P the polarisation propagator as

$$P(\underline{q}_{\parallel},x,x',\omega) = P^{LL}(\underline{q}_{\parallel},\omega)\sum_{g} A^{LL}(x - sa)A^{LL}(x' - sa) + P^{LU}(\underline{q}_{\parallel},\omega)\sum_{g} A^{LU}(x - sa)A^{LU}(x' - sa) \qquad 18$$

where

$$A^{LL}(x - sa) = \phi^{L}(x - sa)\phi^{L}(x - sa) \qquad 19a$$

$$A^{LU}(x - sa) = \phi^{L}(x - sa)\phi^{U}(x - sa) \qquad 19b$$

$$P^{LL} = \frac{2}{\Omega}\sum_{\underline{k}_\parallel} \frac{n_{k_\parallel} - n_{k_\parallel + q_\parallel}}{\epsilon_{\underline{k}_\parallel} - \epsilon_{\underline{k}_\parallel + q_\parallel} - \hbar\omega - i\delta} \qquad 20$$

$$P^{LU} = \frac{2}{\Omega}\sum_{\underline{k}_\parallel} \frac{n_{k_\parallel}}{\epsilon_{\underline{k}_\parallel} - \epsilon_{\underline{k}_\parallel + q_\parallel} - E_g - \hbar\omega - i\delta} - \frac{2}{\Omega}\sum_{k} \frac{n_{k_\parallel + q_\parallel}}{\epsilon_{\underline{k}_\parallel} + E_g - \epsilon_{\underline{k} + q_\parallel} - \hbar\omega - i\delta} \qquad 21$$

$$\epsilon_{\underline{k}_\parallel} = \hbar^2 k_\parallel^2 / 2m. \qquad 22$$

Our calculations have shown that the subbands at least within in the well would be expected to be fairly parallel as in the case of effective mass theory so we take the energy gap between the lower and upper sub-band as a constant. For simplicity we have assumed the $\phi^{(\alpha)}(x)$ to be real functions. The P^{LL} and P^{LU} are just the intra- and inter-band polarisation propagators for a two-dimensional electron gas (35). They correspond to a metallic-like and semiconductor-like polarisation with the polarisation along and across the wells respectively. The A are weighting factors reflecting the three-dimensional character of superlattices and in particular the finite width of the quantum wells. It is the A's which contain the wavefunction of the well and so better approximations for the quantum well states are reflected directly in these terms.

The dielectric response function is now

$$\epsilon(x,x',q_\parallel,\omega) = \delta(x - x') - \sum_{s,\upsilon}\int \frac{2\pi e^2}{q_\parallel} \exp(-q_\parallel |x - x''|)(P(q_\parallel,\omega)A(x'' - sa)^{\upsilon} \qquad 23$$

$$\times(A(x' - sa))^{\upsilon} dx''$$

where υ is an index denoting either LL or LU.

ϵ is the dielectric response function, but it must be remembered that all physical processes involve not ϵ but ϵ^{-1} (through the screened electron–electron interaction). It is misleading therefore to consider ϵ in anything other than the uniform system where ϵ^{-1} is just $1/\epsilon$.

ϵ is now separable in x and x' and can be inverted using an identity for the inverse of a separable matrix (36). Effectively this reduces the problem from one of inverting a matrix over a continuous variable to inverting a matrix with discrete labels.

ϵ^{-1} can be written as (36)

$$\epsilon^{-1}(x,x',q_\parallel,\omega) = \delta(x - x')$$

$$+ \sum_{\substack{s,t \\ \upsilon\upsilon'}} \int \upsilon(q_\parallel,x,x'')(P(q_\parallel,\omega)A(x'' - sa))^{\upsilon} Q_{st}^{\upsilon\upsilon'} (A(x' - ta))^{\upsilon'} dx'' \qquad 24$$

where

$$\left[Q_{st}^{-1}\right]^{\nu\nu'} = \delta_{st}^{\nu\nu'} - \iint (P(q_{\parallel},\omega)A(x - sa))^{\nu} v(q_{\parallel},x,x')A(x' - ta))^{\nu'} dxdx'. \qquad 25$$

The coulombic potential $v(q_{\parallel},x,x')$ falls off exponentially as $\exp(-q_{\parallel}|x - x'|)$ and causes the matrix Q^{-1} to have a tight binding structure.

Since it is a matrix in the subband and well position index the matrix can be inverted for a finite number of wells directly. For instance a 5 well 2 subband system will require the inversion of a 10 × 10 matrix (see also Jain and Allen (37)). For a superlattice, by imposing Born-Von Karman boundary conditions in the superlattice direction, Q^{-1} can be diagonalised and inverted using a unitarity transformation. The algebra is somewhat lengthy but straightforward and we quote only the result:

$$Q_{st}^{\nu\nu'} = \sum_k \frac{e^{iska}}{N} \Gamma^{\nu\nu'}(k,\omega)e^{-ikta} \qquad 26$$

where

$$\Gamma^{-1\nu\nu'} = X^{\nu\nu'} + Y^{\nu\nu'} \frac{\exp(-q_{\parallel}a + ika)}{1 - \exp(-q_{\parallel}a + ika)} + Z^{\nu\nu'} \frac{\exp(-q_{\parallel}a - ika)}{1 - \exp(-q_{\parallel}a - ika)} \qquad 27$$

$$X^{\nu\nu'} = \delta^{\nu\nu'} - P^{\nu}(q_{\parallel},\omega)\frac{2\pi e^2}{q_{\parallel}}\int_{-a/2}^{a/2}\int_{-a/2}^{a/2} A^{\nu}(x)\exp(-q_{\parallel}|x - x'|)A^{\nu'}(x')dxdx' \qquad 28$$

$$Y^{\nu\nu'} = -P^{\nu}(q_{\parallel},\omega)\frac{2\pi e^2}{q_{\parallel}}\int_{-a/2}^{a/2}\int_{-a/2}^{a/2} A^{\nu}(x)e^{qx}A^{\nu'}(x')e^{-qx'}dx'dx \qquad 29$$

$$Z^{\nu\nu'} = P^{\nu}(q_{\parallel},\omega)\frac{2\pi e^2}{q_{\parallel}}\int_{-a/2}^{a/2}\int_{-a/2}^{a/2} A^{\nu}(x)e^{-qx}A^{\nu'}(x')e^{qx'}dxdx' \qquad 30$$

$k = 2\pi n/Na$

where N = number of planes, n = integer, $n \leq N$ and where $(\Gamma^{\nu\nu'})$, $(X^{\nu\nu'})$, $(Y^{\nu\nu'})$and $(Z^{\nu\nu'})$ are all two by two matrices reflecting the fact that we are using a two subband model.

We write as our final expression of ϵ^{-1}

$$\epsilon^{-1} = \delta(x - x') + \sum_{st,k}\sum_{\nu\nu'} \int v(q_{\parallel},x,x'')(P(q_{\parallel},\omega)A(x'' - sa))^{\nu} \frac{e^{iska}}{N^{1/2}} \Gamma^{\nu\nu'} \frac{e^{-ikta}}{N^{1/2}} \qquad 31$$

$$\times (A(x' - ta))^{\nu'} dx''$$

The plasmon modes are easily found by noting that they are at the frequency poles of ϵ^{-1} (30-33). These occur when

$$(\Gamma^{-1})^{11}(\Gamma^{-1})^{22} - (\Gamma^{-1})^{12}(\Gamma^{-1})^{21} = 0. \qquad 32$$

It must be noted that that plasmon dispersion curve depends implicitly on the microscopic form of the subband wavefunctions through equation (32). Thus for any model of these states we will obtain the appropriate plasmon modes.

The screened electron-electron interaction, just as in the bulk, can be thought of in terms of containing a part due to plasmon exchange which reduces the bare Coulomb (photon-exchange) term. Thus we write

$$w = \epsilon^{-1} v - v + \sum_{\nu} \gamma^{\nu}_{e-p} D^{\nu}_{plasmon} \gamma^{\nu}_{ep} \qquad 33$$

where γ^{ν}_{e-p} and $D_{plasmon}$ are the electron-plasmon coupling and the plasmon propagator for the mode ν. Looking at equation (31) we see this structure very clearly, the modes being determined essentially by $P\Gamma$ while the spatial parts give the electron-plasmon coupling. Ignoring the off-diagonal terms in Γ the screened interaction splits into the exchange of two plasmons associated with inter- and intra-subband excitations. The off-diagonal terms introduce mixing between the modes but because the two plasmon bands generally have very different energies the couplings are very small.

B3 Results

Using these expressions the plasmon dispersion relationship for a typical superlattice is given in figure (14). These results have used a single sine and cosine form for the well wavefunction so as to compare with the expression of Bloss (30) and Tselis and Quinn (33) for the upper band and Giuliani, Qin and Quinn (32) for the lower in the appropriate limit. We also show the electron hole continuum inter- and intra-band excitations. The two modes are basically a 'metallic'-like intra-subband mode and a 'semiconductor'-like inter-subband mode. The bands shown are the range of plasmon energies for varying the momentum perpendicular to the layers. For a finite series of wells we would get a finite set of curves lying within the two bands.

The plasmons are quite clearly outside these regions and so will be long lived modes. In particular the upper plasmon band is always found to be above the interband excitation spectrum because of the effect of the poles in the polarisation term P^{LU}.

We find that the gross features of the plasmon spectrum are basically independent of the well widths, occupation etc simply scaling as one would expect with electron density, inter-subband separation etc. The results for a superlattice give a band of plasmon energies each governed by the perpendicular component of momentum. For a set of wells the result would be a finite series of plasmon bands as seen for instance in the experimental work of Pasol et al (38).

We have investigated the effect of finite transverse fields on the plasmon modes since any surface oriented device would be expected to utilise gate voltages to modify the electron density. Even without

changes in electron density however there are marked changes in the upper "interband" plasmon properties. Figure (15) shows such a field dependence for a single well. The main effect arises through the polrisation P^{LU} from the change in the interband energy as the transverse field increases as can be seen from the single particle spectrum. But the wavefunctions in the well are altering significantly as well as changing the interplasmon coupling terms $[(\Gamma^{-1})^{12}, (\Gamma^{-1})^{21}]$ through the changes in A.

B4 Summary

The above work represents a simple scheme for evaluating the plasmon modes and matrix elements for electron plasmon coupling for any combination of quantum well properties. The level of approximation being simply set by the sophistication of the evaluation eigenstates (through the A's) and subband energies (through the P's). There is no restriction on quantum well or subband numbers other than the size of matrix required. We believe this technique has significant advantages over the others in the literature not least through its' direct connection to the screened interaction in the quantum well system which enables direct calculation of all electron-electron interaction based terms.

III SUMMARY

The possibilities for microscopic device design utilising the submicron geometries possible with heterojunction technologies are almost endless (1,2,25,26,27). It is important therefore to consider carefully the consequences of our work in a device context.

i Effective Mass Theory: we have shown that for eigenvalues, transmission and reflection coefficients, what we have described as EMT2 (equation 14) does remarkably well with the following provisos:

a the Γ to Γ band offset must be used;

b non parabolicities of the band structure both real and complex need to be taken into account as in Bastards (22) model;

c the energies considered must be well below any of the higher minima.

This means that for low field devices the standard methods of EMT can be used with some confidence.

ii Intervalley Transfer: Our calculations show strong intervalley transfer due to scattering at the interface once the electron energy becomes high enough. Figures 10 and 11 show quite clearly that in any hot electron quantum well based device, intervalley transfers will contribute substantially to any I-V characteristic. The staircase (27) and CHIRP (25,26) structures are obvious examples. It should also be noticed that the process in any intervalley transfer based device (such as a GUNN diode) will be severely modified on going to a quantum well structure. It is quite conceivable that the intervalley transfer rate due to interface scattering could dominate over phonon induced processes in a narrow well. This would significantly alter peak to valley ratio and frequency range.

iii Plasmons: our calculations have shown that it is possible to calculate both the plasmons and the electron-electron interaction for realistic well widths, subband structure and finite sized systems. The calculation of the effect of electric field on the plasmons is important because in any surface oriented device significant transverse electric fields are expected. Although the lower plasmons are fairly sensitive to such fields the upper band plasmons vary very strongly.

iv Electron-Plasmon Interaction: the concentration to date has been on the properties of plasmons, (30,31,32,33,37). However the crucial aspect from a device standpoint is the interaction of those plasmons with electron states. We have not yet performed such calculations but the formulation is in place through a combination of equations (31) and (19). The important point to realise is that the matrix elements for the excitation of the lower plasmon are quite different from that of the upper one. In

essence the lower plasmon cannot cause inter-subband scattering whilst the upper plasmon cannot cause intra-subband scattering. This means that their effect on the dynamics of the electron system is qualitatively different.

v Electron-Phonon Interaction: the standard calculations of conductivities, electron loss etc via phonon scattering are based on effective mass considerations. In particular it is well known that for electrons scattering within one minimum, only zone centre optical phonons are really important. The calculations presented in Section A show, however, that the scattering from an interface excites large amplitude states characteristic of the higher minima. If this is so then any state in a quantum well or superlattice system will have a mixture of characteristics from a number of minima. This means that any electron phonon matrix will couple not only the zone centre phonons but also zone edge phonons. For narrow well systems these could be a substantial contribution to the scattering producing a marked decrease in the mobility no matter how perfect the interface.

vi Plasmon-Photon Interaction: The generation of radiation in any free electron laser type of device (3) must be through plasmon photon coupling. The formulation of Section B can be modified to treat the transverse response of a quantum well system which describes such coupling. We are at present in the process of doing just this and it will be complete within the next two months. A copy of the resulting publication will be sent to ERO.

There are a large number of possibilities for further work, some of which we have already started.

a The extension to other materials and strained lattices. This requires little extra work since the pseudopotential coefficients are well-known as are the lattice parameters. The method is sufficiently flexible and accurate to give results for any of the practical material calculations. There are many interesting possibilities in studying the more exotic materials combinations using our method, since the alternative tight binding based methods simply do not have the accuracy required. The effect of strain on the higher minima or in Si and Ge the degenerate sets of conduction band minima will automatically be included.

b Valence Band Effects: We have deliberately concentrated upon the conduction bands, the valence bands can, however, be treated similarly in our method by simply moving to the appropriate energy range of interest.

c Incorporation of electric fields in the electron scattering matrix formulation. With this extension we will be able to treat realistic device potential profiles resulting from space charge effects and also look at I-V characteristics.

d Dynamics of plasmon hot electron systems: this is really the application of Sections A and B to the free electron laser system.

e Plasmon Photon Coupling

In conclusion we have presented in this report an extensive volume of work of central interest to submicron device design. This is being continued to understand the microscopic behaviour of a whole range of quantum well systems.

Acknowledgement

This work would not have been possible without the able assistance of my research collaborators, in particular A C Marsh and D King-Smith.

IV REFERENCES

1 Grubin H L, Hess K, Iafrate G J, Ferry D K (eds), Physics of Submicron Structures, Plenum, 1984.

2 Bauer G, Kucher F, Heinrich H (eds), Two Dimensional Systems, Heterostructures and Superlattices, Springer Verlag, 1984.

3 Marshall T C, Free Electron Lasers, Macmillan, 1985.

4 Marsh A C and Inkson J C, J Phys C: Solid State Physics 17, p6561, 1984.

5 Marsh A C and Inkson J C, J Phys C: Solid State Physics 19, p43, 1986.

6 Marsh A C and Inkson J C, IEEE J Quantum Electron QE-22, p58, 1986.

7 Marsh A C and Inkson J C, Semicond Sci Technology 1, 1986, pp285-290.

8 Marsh A C and Inkson J C, Solid State Commun, Vol 52, pp1037-1039, 1984.

9 Pickett W E, Louie S G and Cohen M L, Phys Rev B17, p815, 1978.

10 Wong K B, Jaros M. Gell M A and Ninno D, J Phys C: Solid State Phys 19, p53, 1986.

11 Osborn G C and Smith D L, Phys Rev B19, p2124, 1979.

12 Schulman J N and Chang Y C, Phys Rev B31, p2056, 1985.

13 Heine V, Proc Phys Soc, Vol 81, pp300-310, 1963.

14 Inkson J C, J Phys C: Solid State Phys 13, pp369-381, 1980.

15 Burt M G and Inkson J C, J Phys D: Appl Phys 9, p43, 1976.

16 Pendry J B, Low Energy Electron Diffraction (London: Academic Press) 1974

17 Cohen M L and Bergstrasser T K, Phys Rev 141, p798, 1966.

18 Baldereschi A, Hess E, Maschke K, Neumann H, Schulze K R and Unger K, J Phys C: Solid State Phys 10, p4709, 1977.

19 Tsu R and Esaki L, Appl Phys Lett 22, p562, 1973.

20 Marsh A C, IEEE J Quantum Electron. Submitted.

21 Marsh A C, Semicond Sci Technol 1, p237, 1986.

22 Bastard G, Superlattices and Microstructures 1, p265, 1985.

23 Schulman J N, J Vac Sci Technol B, Vol 1, pp644-647, July 1983.

24 Lee J, Vassell M O, Lockwood H F, in Ref 1, p33.

25 Nakagawa T, Kawai N J and Ohta K, Superlattices Microstruct 1. p187, 1985.

26 Nakagawa T, Kawai N J, Ohta K and Kawashima M, Electron Lett 19, p822, 1983.

27 Capasso F, J Vac Sci Technol 2, p457, 1983.

28 King-Smith R D and Inkson J C, J Phys C 19, L15, 1986.

29 King-Smith R D and Inkson J C, Phys Rev B33, p5489, 1986.

30 Bloss W L, Solid State Commun 46, p147, 1983.

31 Das Sarma S and Quinn J J, Phys Rev B25, p7603, 1982.

32 Giuliani G F, Qin G and Quinn J J, Fifth International Conference on Electronic Properties of Two Dimensional Systems, p479, 1983, (unpublished).

33 Tselis A C and Quinn J J, Phys Rev B29, p3318, 1984.

34 Hedin L and Lundqvist S, Solid State Phys 23, p1, 1969.

35 Stern F, Phys Rev Lett 18, p546, 1967.

36 Ortuno M and Inkson J C, J Phys C: Solid State Phys 12, p1065, 1979.

37 Jain K and Allen P B, Phys Rev Lett 54, p947, 1985.

38 Pasol G, Mestres N, Hughes H P, Fischer A and Ploog K, Phys Rev Lett 56, no 23, p2517, 1986.

39 Frensley W R and Kroemer H, Phys Rev B16, p2642, 1977.

40 Harrison W A, J Vac Sci Technol 14, p1016, 1977.

41 Waldrop J R, Kawalcyzk K, Grant R W, Kraut E A and Miller D L, J Vac Sci Technol 19, p573, 1981.

42 Dingle R, Weigmann W and Henry C H, Phys Rev Lett 33, p827, 1974.

V FIGURE CAPTIONS

1a A schematic illustration of the effective mass approximation (EMT) in real space. In this approximation only one tunnelling (or evanescent) state may exist in the AlGaAs.

1b The real and complex bandstructures of GaAs and AlGaAs in the EMT approximation. The full lines represent the real bandstructure (assumed parabolic) and the broken lines correspond to complex k_1 values. An eletron in state $|k\rangle$ is considered to be incident on the AlGaAs.

2 The calculated (100) complex bandstructure for the heterojunction interface. The diagram provides a convenient graphical illustration of all the solutions to the three dimensional Schroedinger equation.

3 States in the scattering matrix formulation.

4 Illustration of valence band discontinuities for the GaAs-$Ga_{1-x}Al_xAs$ heterojunction. Theoretical curves: (1) Prensley and Kroemer (39) (111) self-consistent pseudopotential; (2) Marsh and Inkson (111) empirical pseudopotential; (3) Pickett *et al* (9) (110) self-consistent potential; (4) Harrison (40) (111) local combination of atomic orbitals. Experimental points: Waldrop *et al* (41) (110); Dingle *et al* (42) (100). Note: Experimental and computational errors are negligible apart from Pickett *et al* (9) where it is estimated at ± 150 meV. Waldrop *et al* (41) found a strong dependence on conditions of MBE growth.

5 The excitation amplitudes of the major evanescent states on the alloy side of the heterojunction. The result is for an alloy concentration of x=1. Arrows indicate the positions of the various energy minima.

6 Evanescent state contributions on the GaAs side of the junction. Note the amplitude of the Γ_1 state is equal to unity for energies below the top of the well.

7 A graphical solution of equation (12) for the lowest boundstate. Here, the numerical phase shift together with EMT(1) and EMT(2) are shown. The intersection of the curves yield the boundstate energies in the three formalisms. The illustration is for a well width of 50 Å and an alloy concentration of x=0.25.

8 The eigenvalues of an isolated AlAs/GaAs/AlAs quantum well for widths between ~ 5 and 50 Å Results from the parabolic (.....), non-parabolic (- - -) and pseudopotential (———) formalisms are illustrated.

9 The *S*-matrix formalism is applied to the geometry illustrated. A novel feature of the device is the positions of the X_1 minima which form two potential wells for electrons. To concentrate attention on the central region the widths of the confining barriers have been kept constant and the width of the central region (W) has been varied between ~ 6 and 71 Å.

10 The current transmission probability through the structure of figure (9) for W: - 11 Å. The pseudopotential results are compared to the estimates from a parabolic one-band effective-mass model. For convenience, the positions of the resonances have also been indicated.

11 As for Figure 10, except W = 45 Å

12 The positions of the Γ resonances as a function of energy and central well widths of - 11, 23, 34, 45, 56, 68 and 71 Å. The positions of the Γ peaks have been compared to the EMT model. The effective-mass result always gives the higher curve. Some resonances which are close to the top of the well re not predicted in EMT.

13 The transmission probabilities T_X, T_Γ for a well width - 11 Å. The resonances due to the influence of the X valleys can clearly be seen. Note that at the Γ resonance energy unity transmission is not predicted.

14 Theoretical calculation of the plasmon dispersion relation of a superlattice. The frequency is expressed in units of classical plasma frequency. The lowest band represents the region where it is possible for an electron to undergo a real excitation process within the conduction band. The next band shows the plasmon dispersion relation resulting from the lower subband. The third curve is for real excitations across the gap. The final band shows the inter-subband plasmon dispersion relation.

15 Theoretical calculation of the intersubband plasmon dispersion relation of a single quantum well as a function of applied electric field. The parameters used for the illustration are: well width = 50 Å, $m_n^* = 1$, electron density = 10^{16} electrons/m^2.

EMT

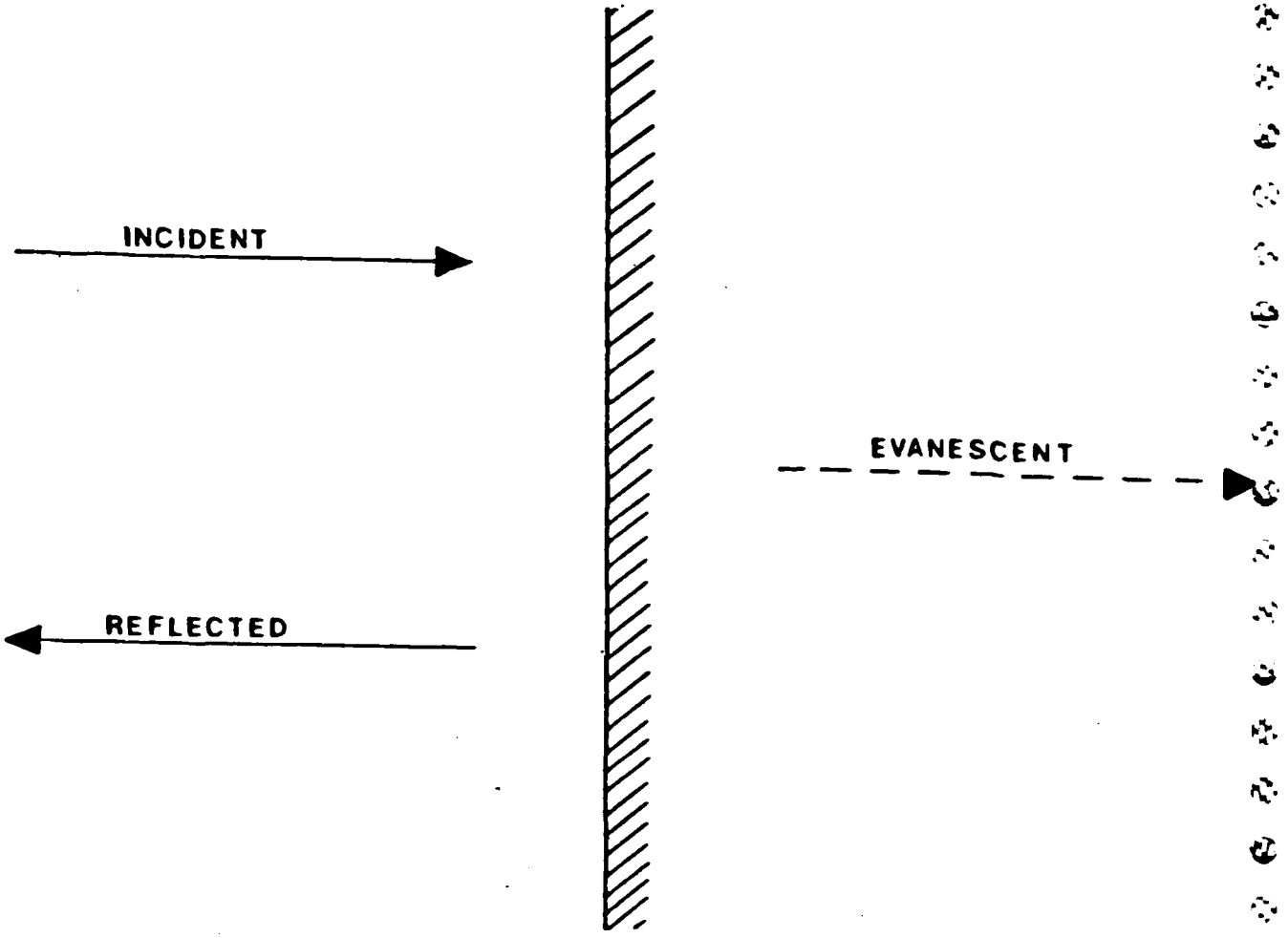

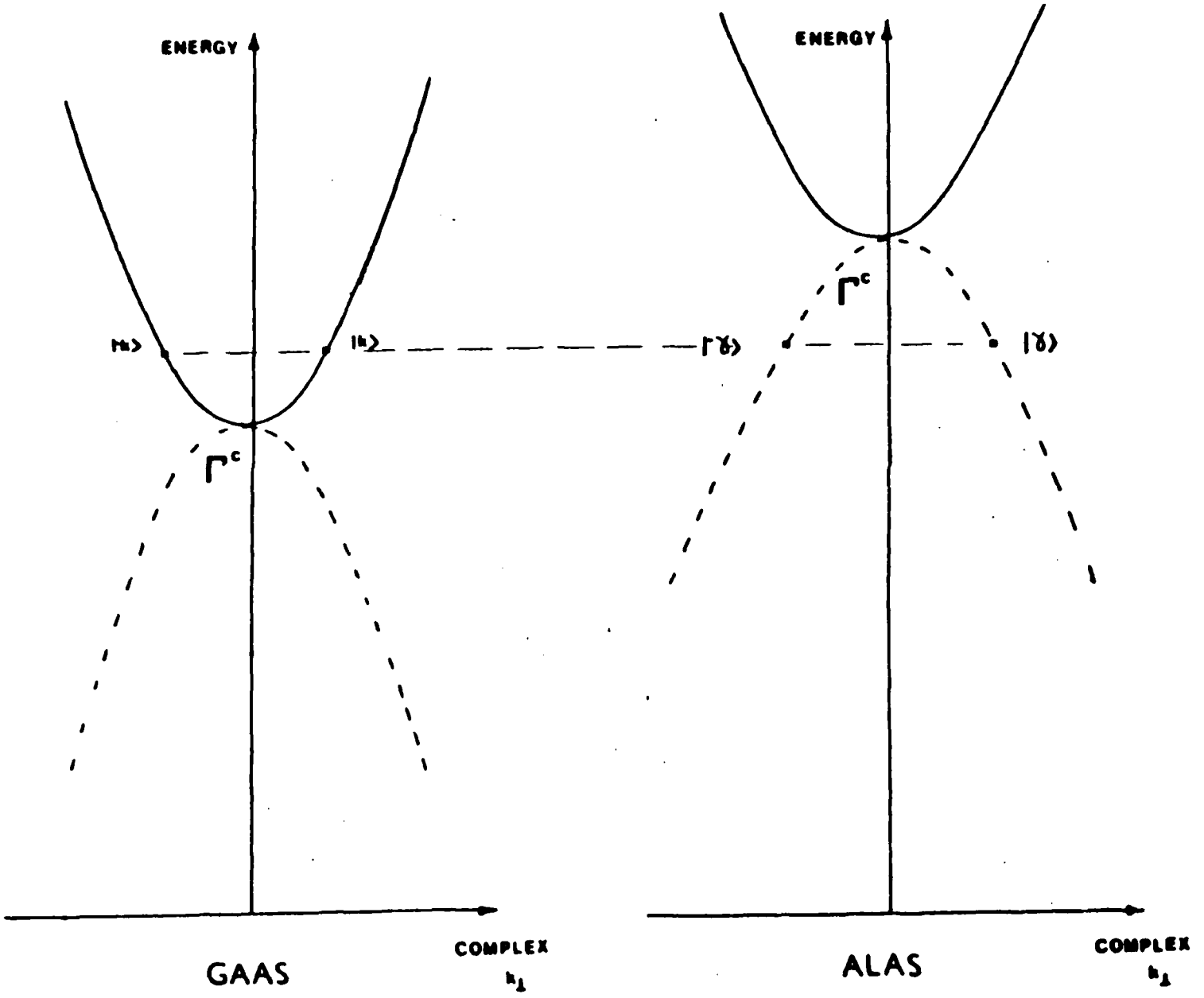
ENERGY
|h>
|l>
Γc
GAAS
COMPLEX
k⊥
ENERGY
|γ>
|g>
Γc
ALAS
COMPLEX
k⊥

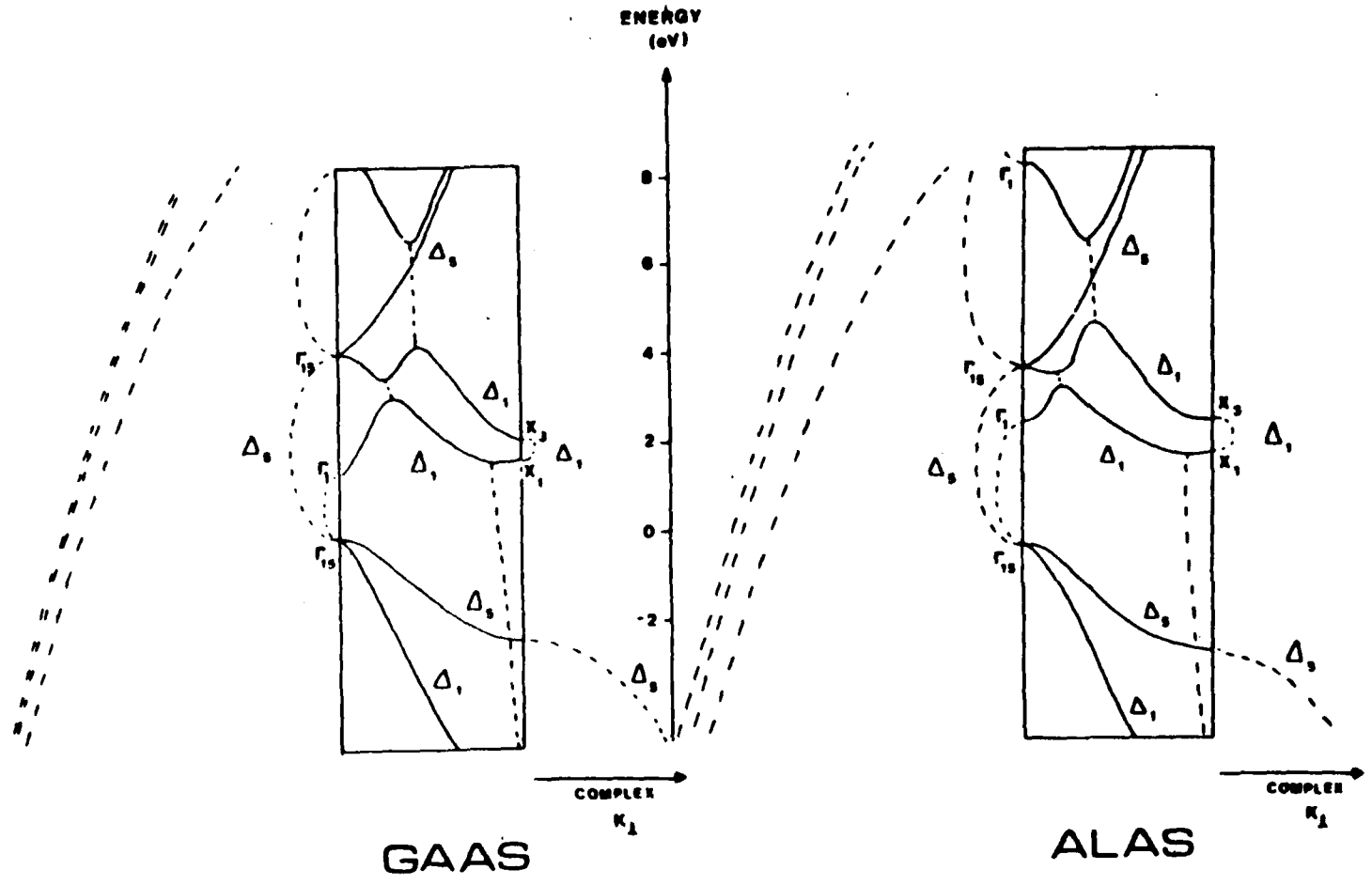

A

B

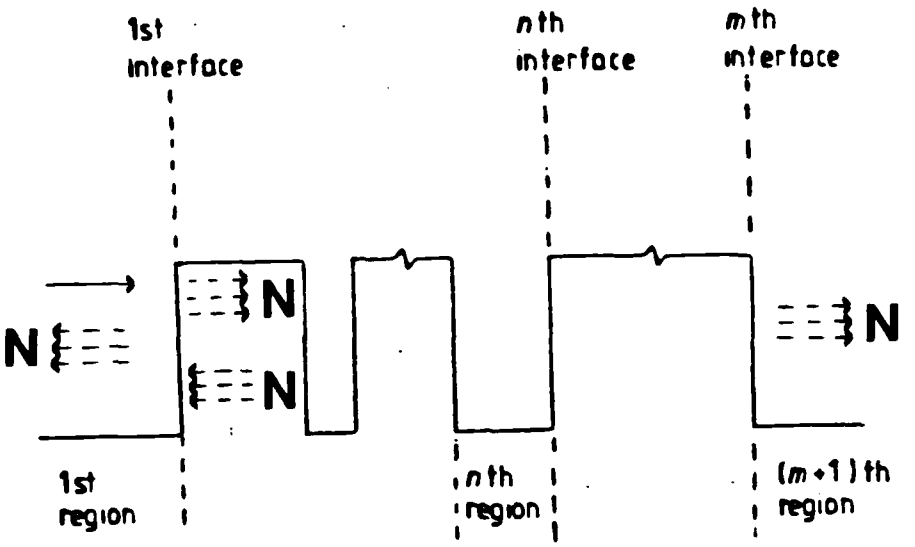
1st
interface
nth
interface
mth
interface
N
N
N
N
1st
region
nth
region
(m+1)th
region

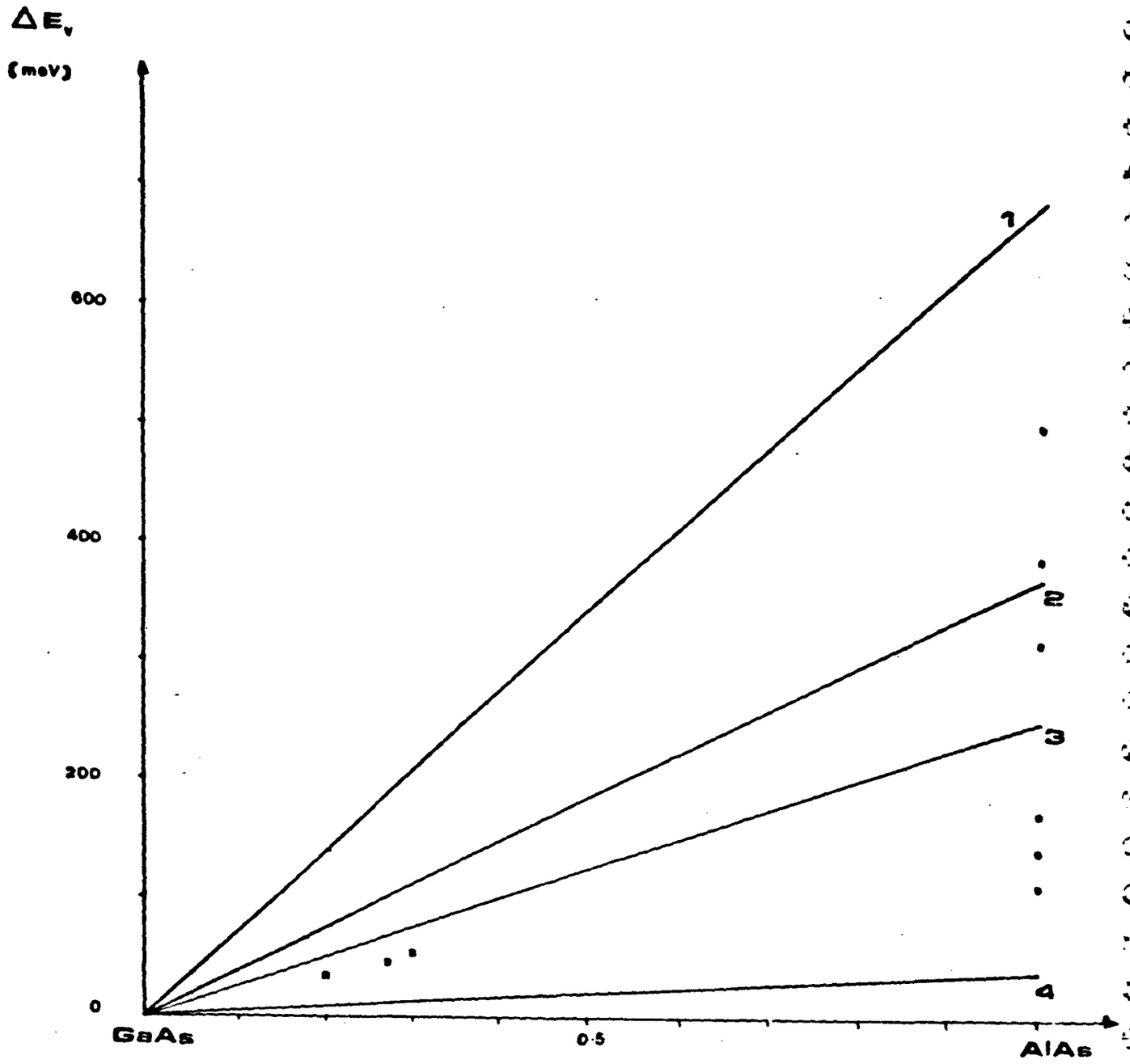
ΔE_v
(meV)
600
400
200
0
1
2
3
4
GaAs
0·5
AlAs

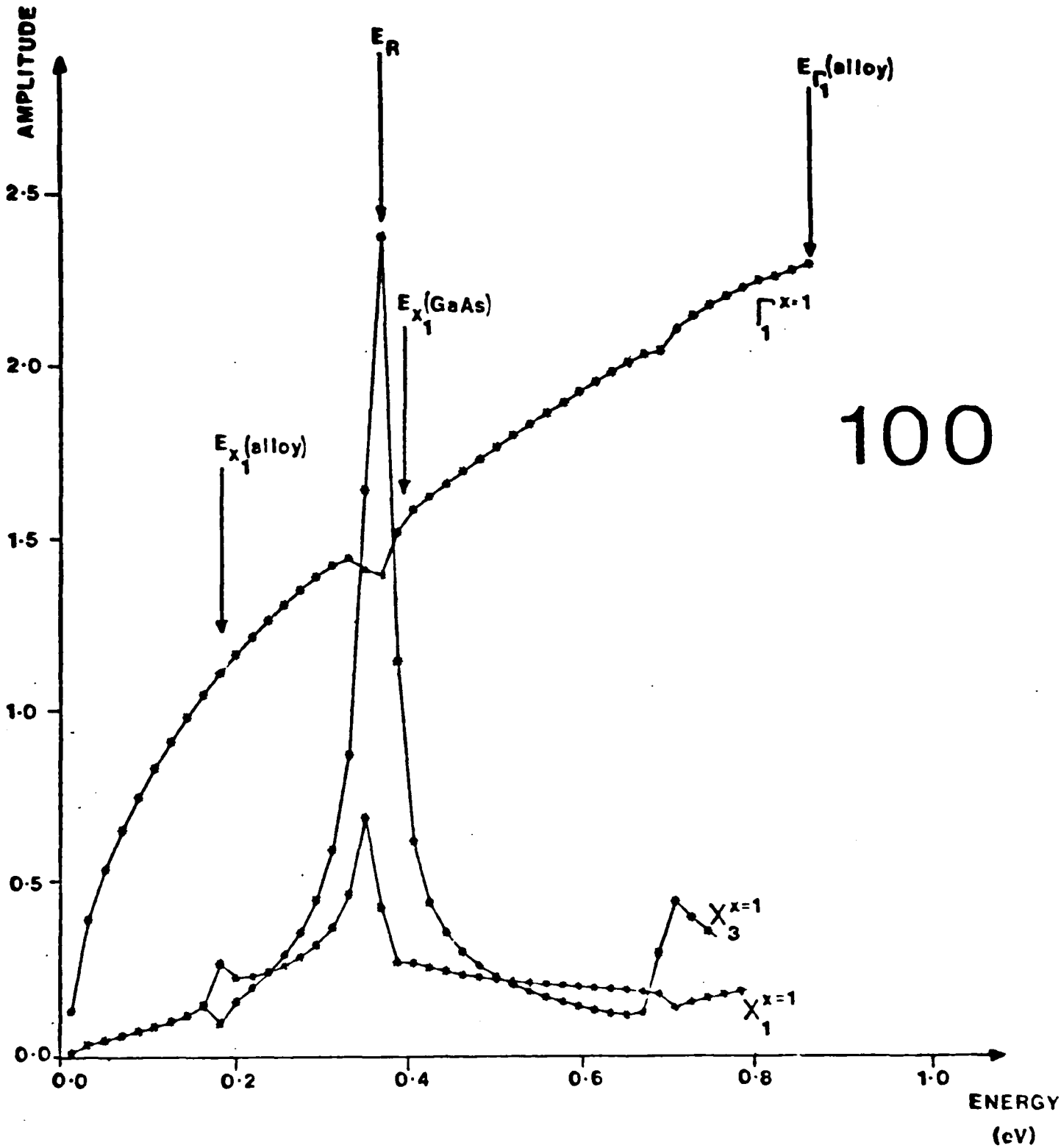
AMPLITUDE
2·5
2·0
1·5
1·0
0·5
0·0
0·0
0·2
0·4
0·6
0·8
1·0
ENERGY
(eV)
E_R
E_{Γ_1}(alloy)
E_{X_1}(GaAs)
$\Gamma_1^{x=1}$
E_{X_1}(alloy)
$X_3^{x=1}$
$X_1^{x=1}$
100

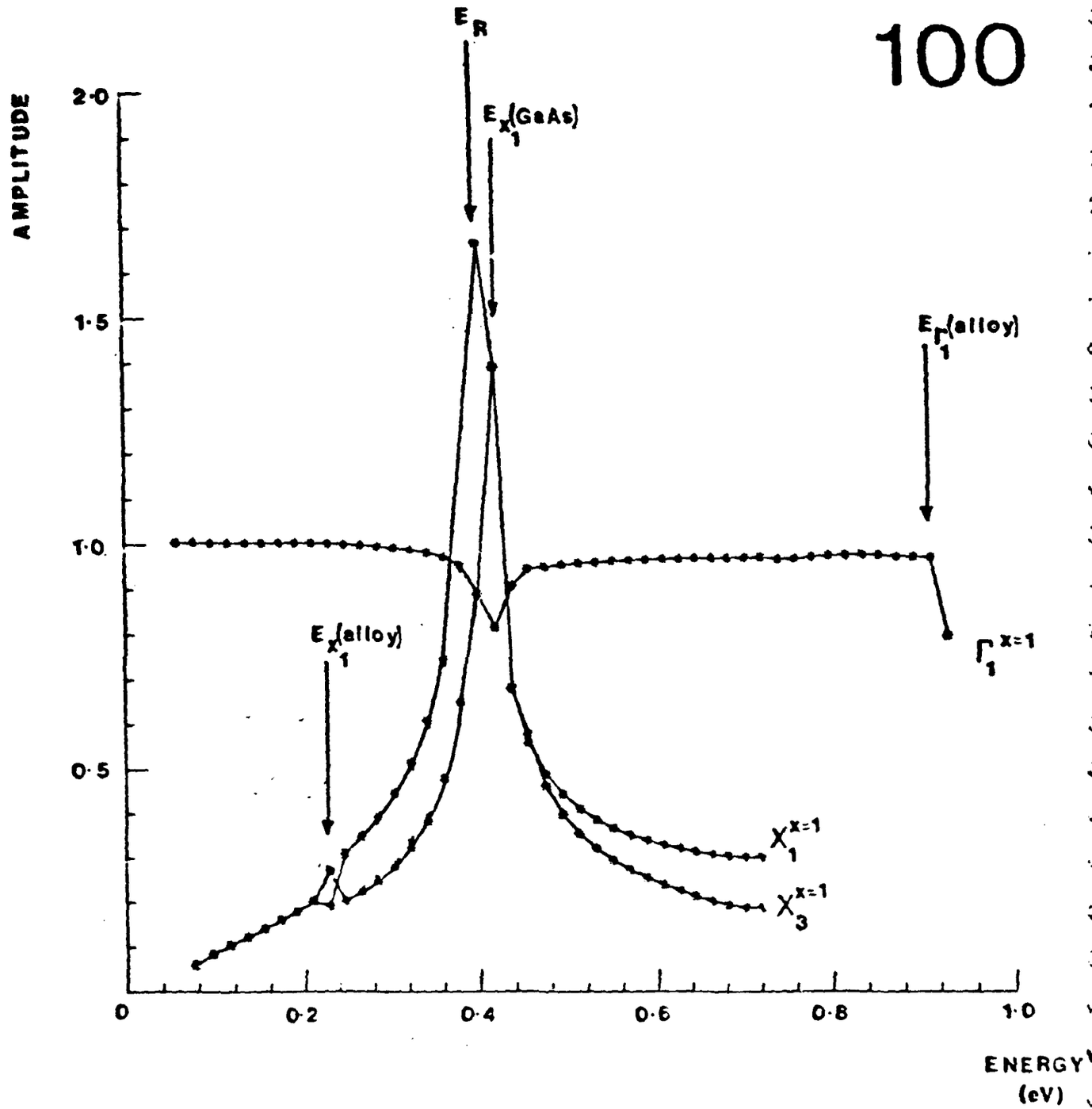
100
E_R
E_{X_1}(GaAs)
E_{Γ_1}(alloy)
E_{X_1}(alloy)
$\Gamma_1^{x=1}$
$X_1^{x=1}$
$X_3^{x=1}$
AMPLITUDE
2·0
1·5
1·0
0·5
0
0·2
0·4
0·6
0·8
1·0
ENERGY
(eV)

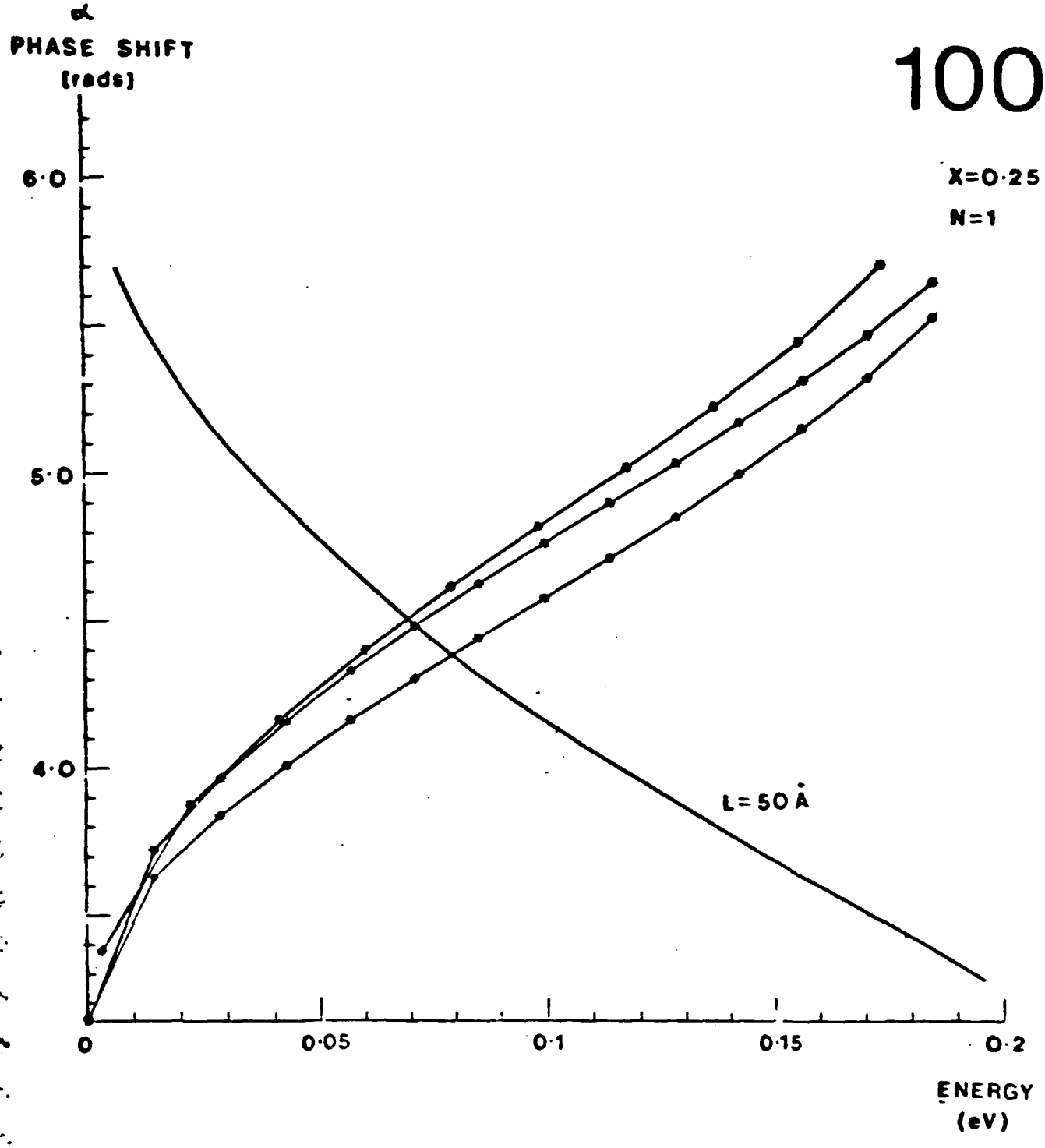
α
PHASE SHIFT
[rads]
100
X=0·25
N=1
6·0
5·0
4·0
L=50 Å
0
0·05
0·1
0·15
0·2
ENERGY
(eV)

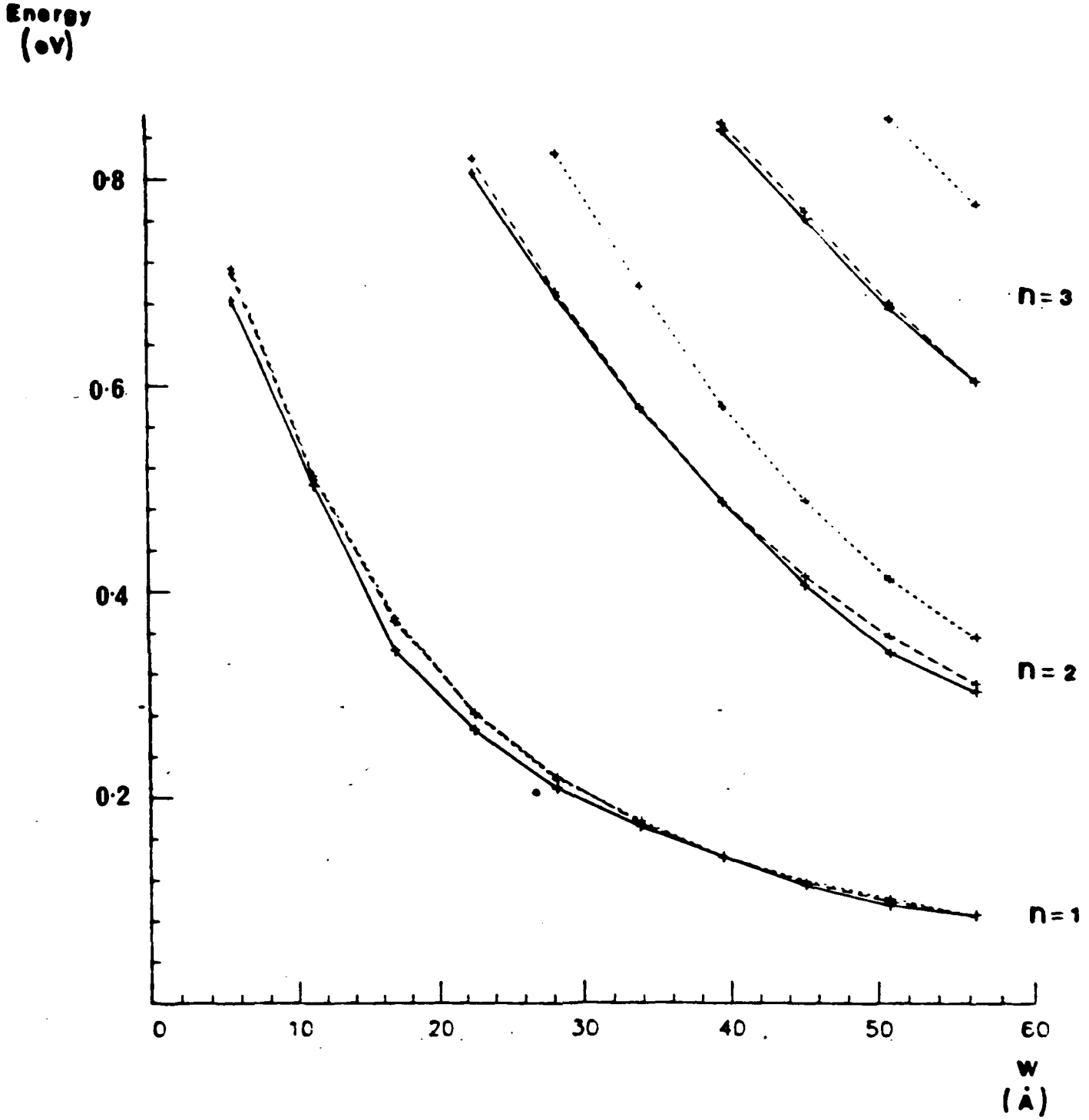
Energy
(eV)
0·8
0·6
0·4
0·2
n = 3
n = 2
n = 1
0
10
20
30
40
50
60
W
(Å)

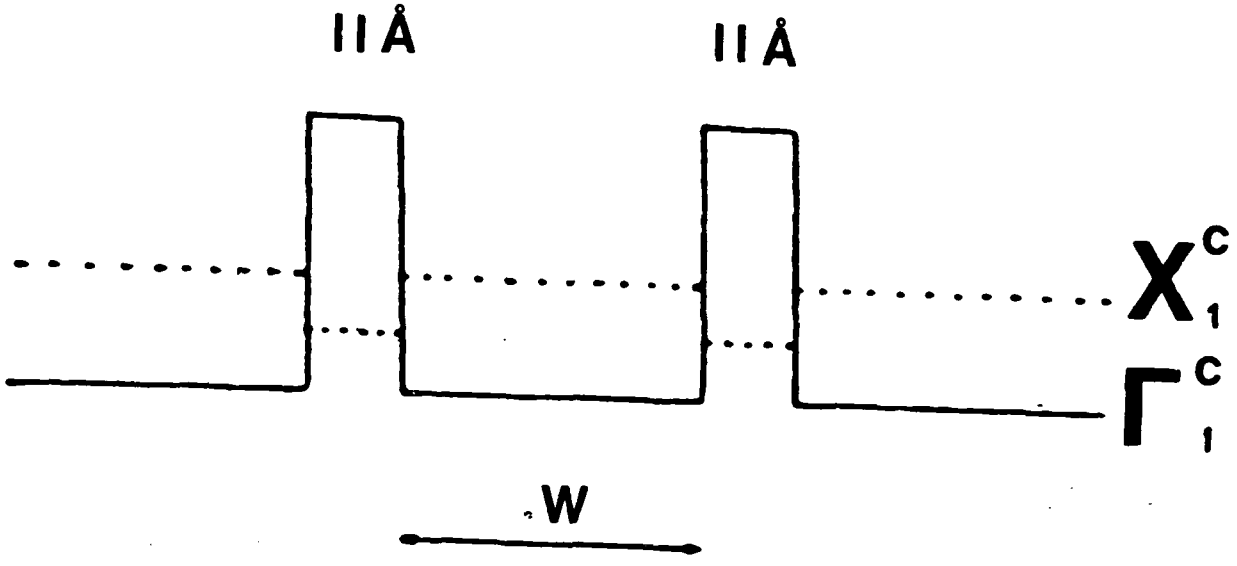
11Å
11Å
X_1^c
Γ_1^c
W

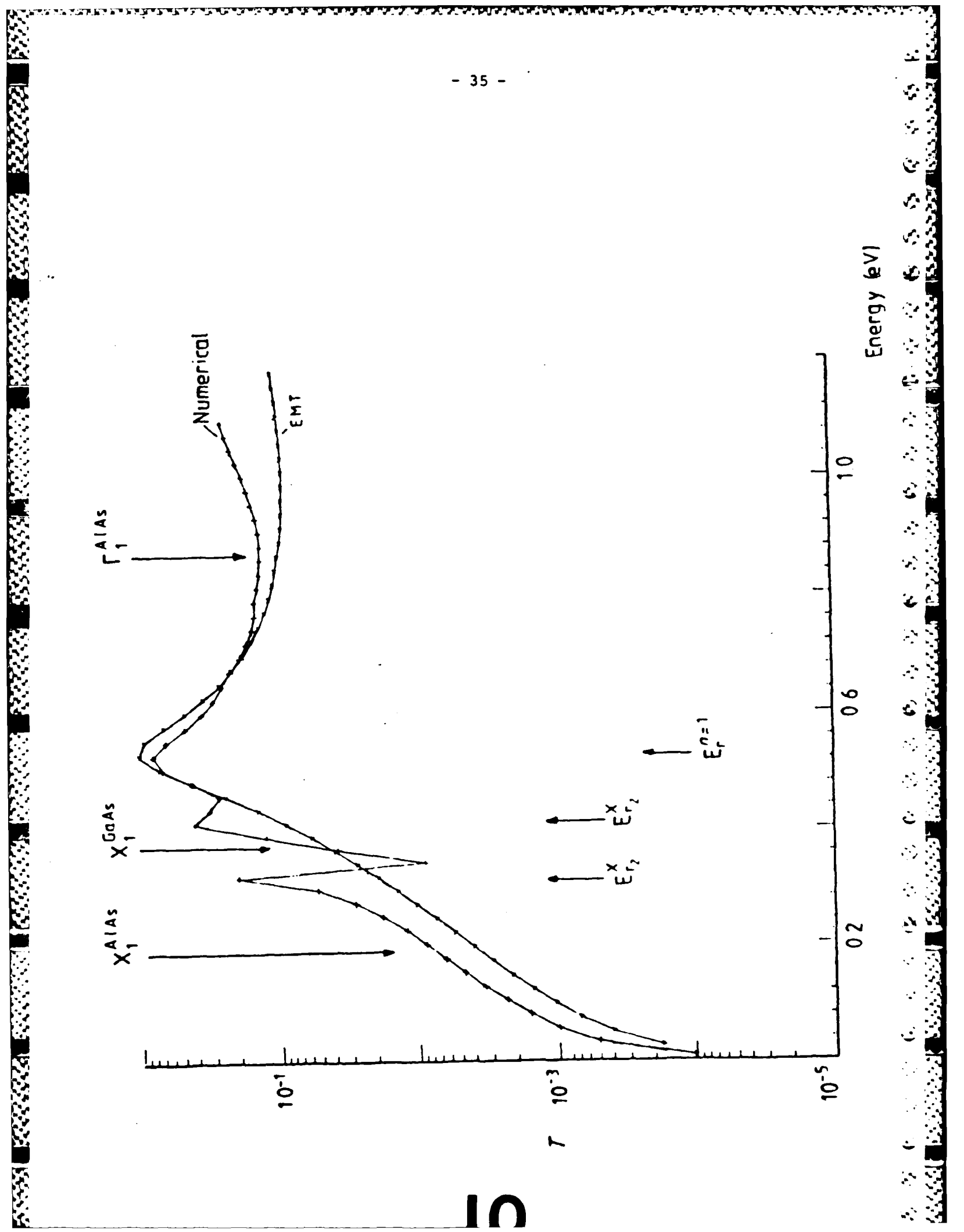
Numerical
EMT
Γ_1^{AlAs}
X_1^{GaAs}
X_1^{AlAs}
$E_{\Gamma_2}^{X}$
$E_{\Gamma_2}^{X}$
$E_\Gamma^{n=1}$
T
10^{-1}
10^{-3}
10^{-5}
0 2
0 6
1 0
Energy (eV)

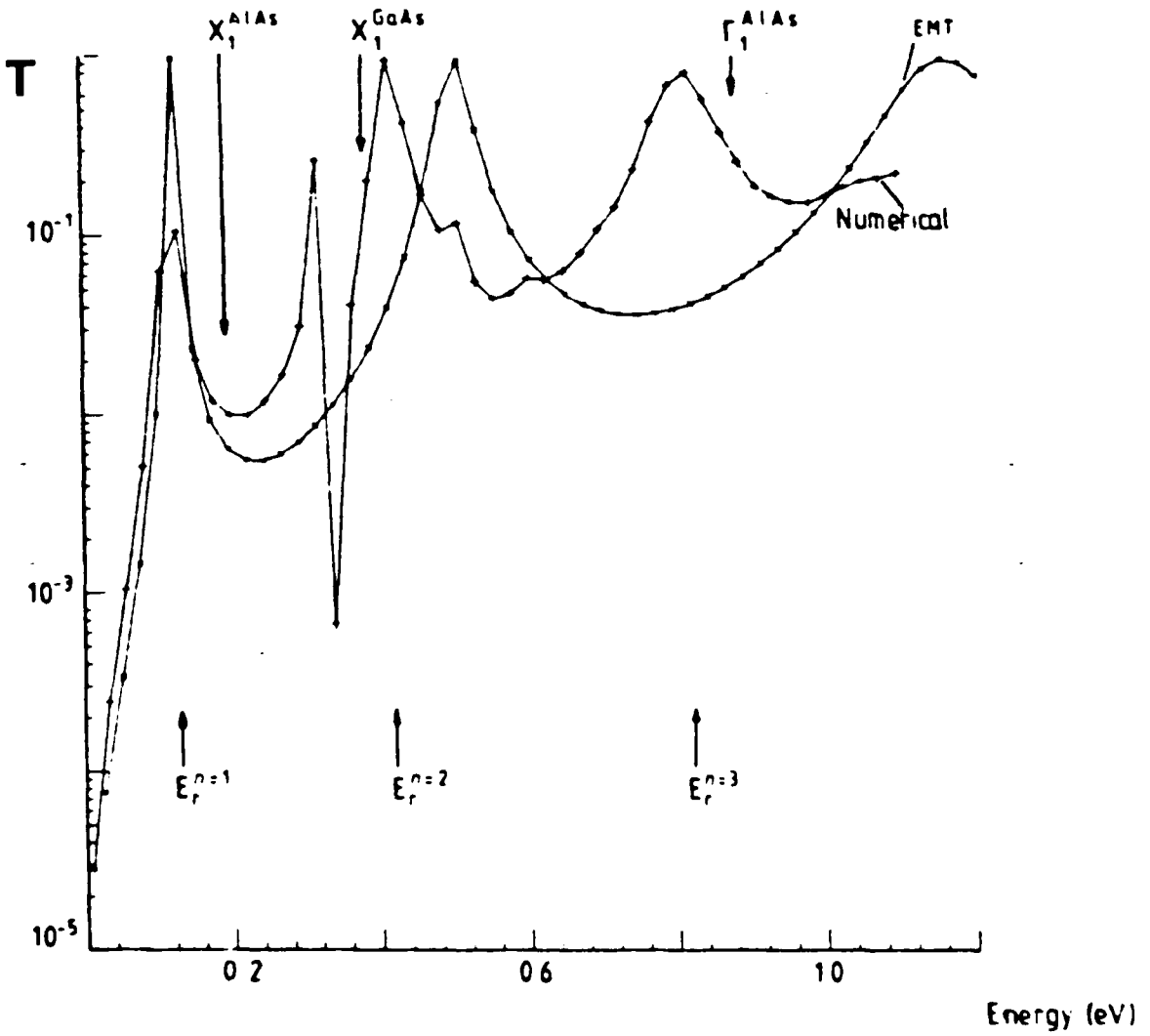
T
X_1^{AlAs}
X_1^{GaAs}
Γ_1^{AlAs}
EMT
Numerical
10^{-1}
10^{-3}
10^{-5}
$E_r^{n=1}$
$E_r^{n=2}$
$E_r^{n=3}$
0 2
0 6
1 0
Energy (eV)

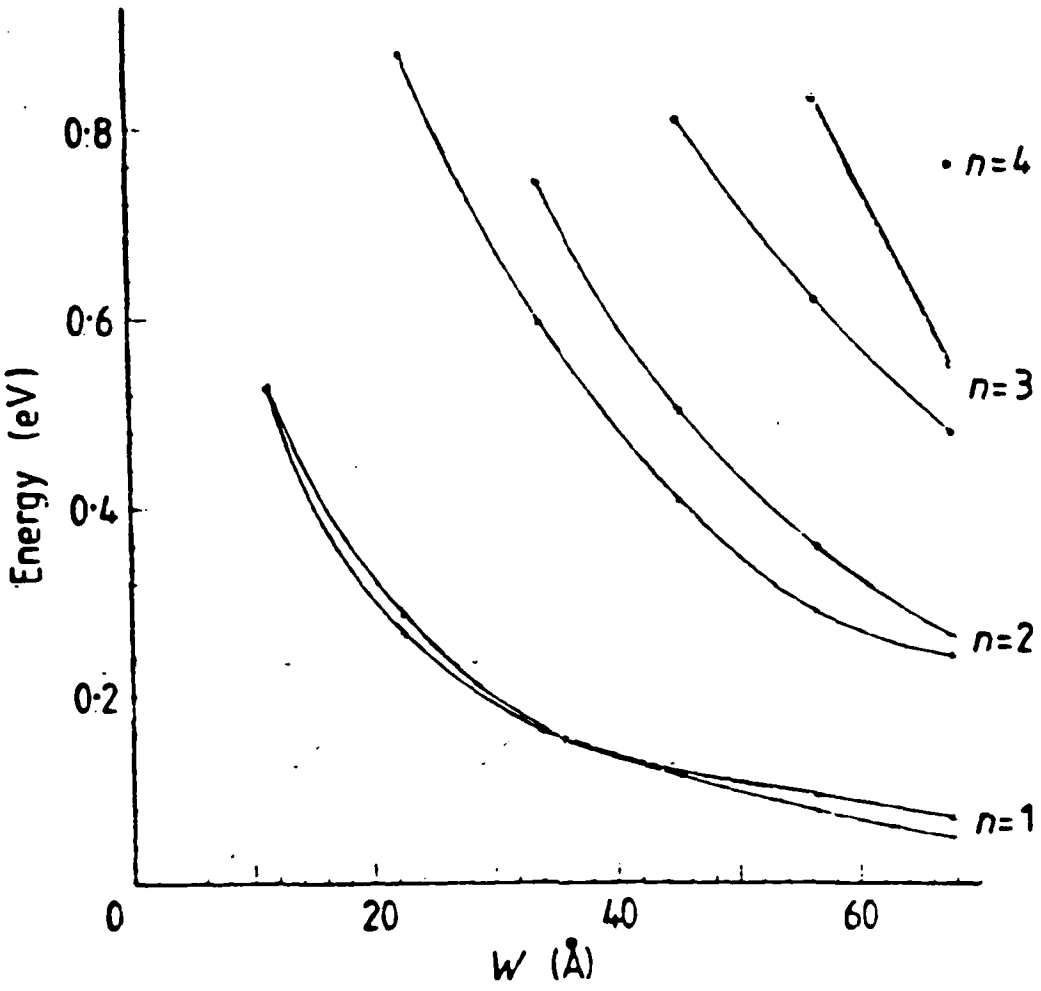
0·8
0·6
0·4
0·2
Energy (eV)
0
20
40
60
W (Å)
n=4
n=3
n=2
n=1

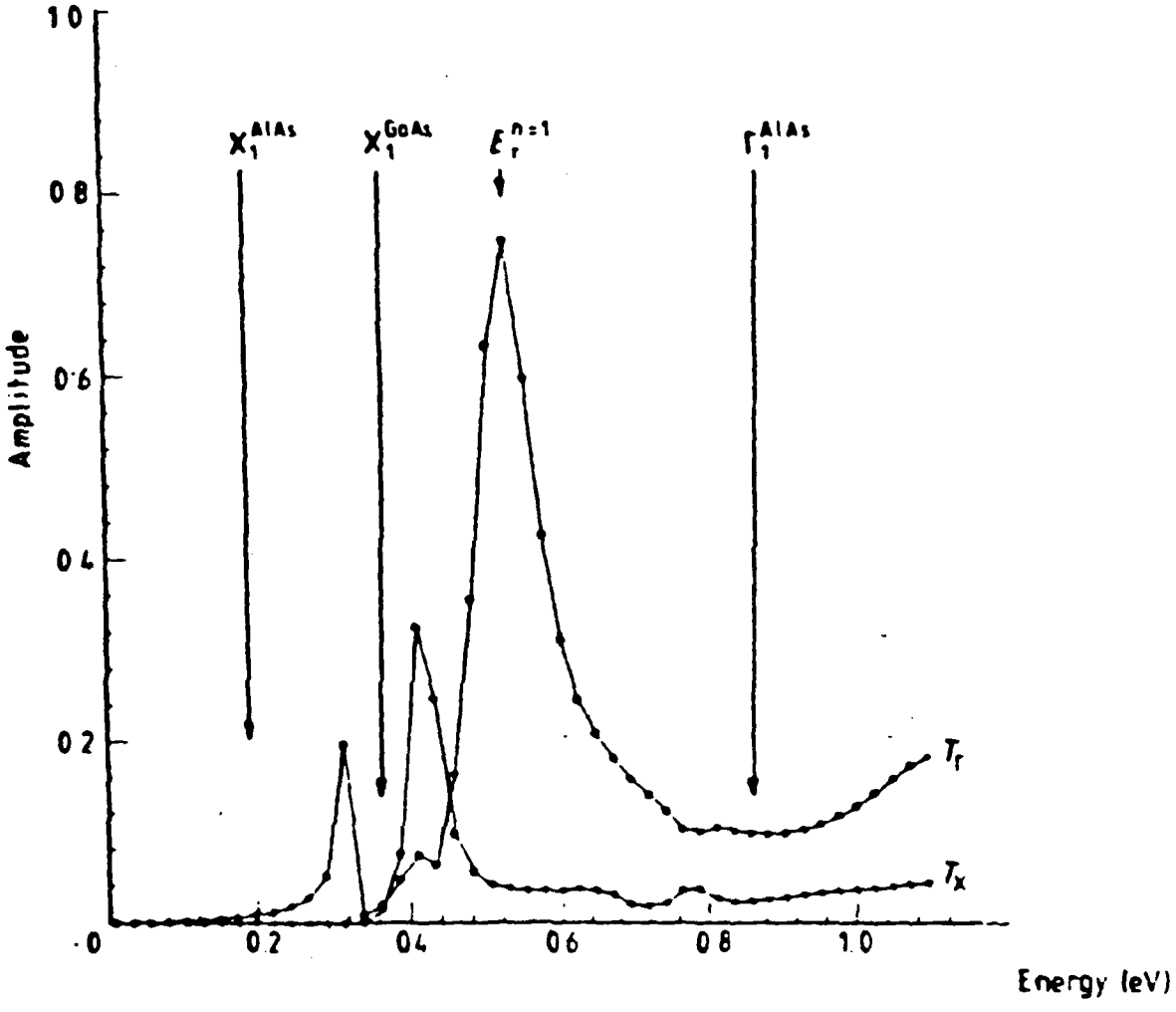
1.0
0.8
0.6
0.4
0.2
0
Amplitude
X_1^{AlAs}
X_1^{GaAs}
$E_\Gamma^{n=1}$
Γ_1^{AlAs}
T_Γ
T_X
0.2
0.4
0.6
0.8
1.0
Energy (eV)

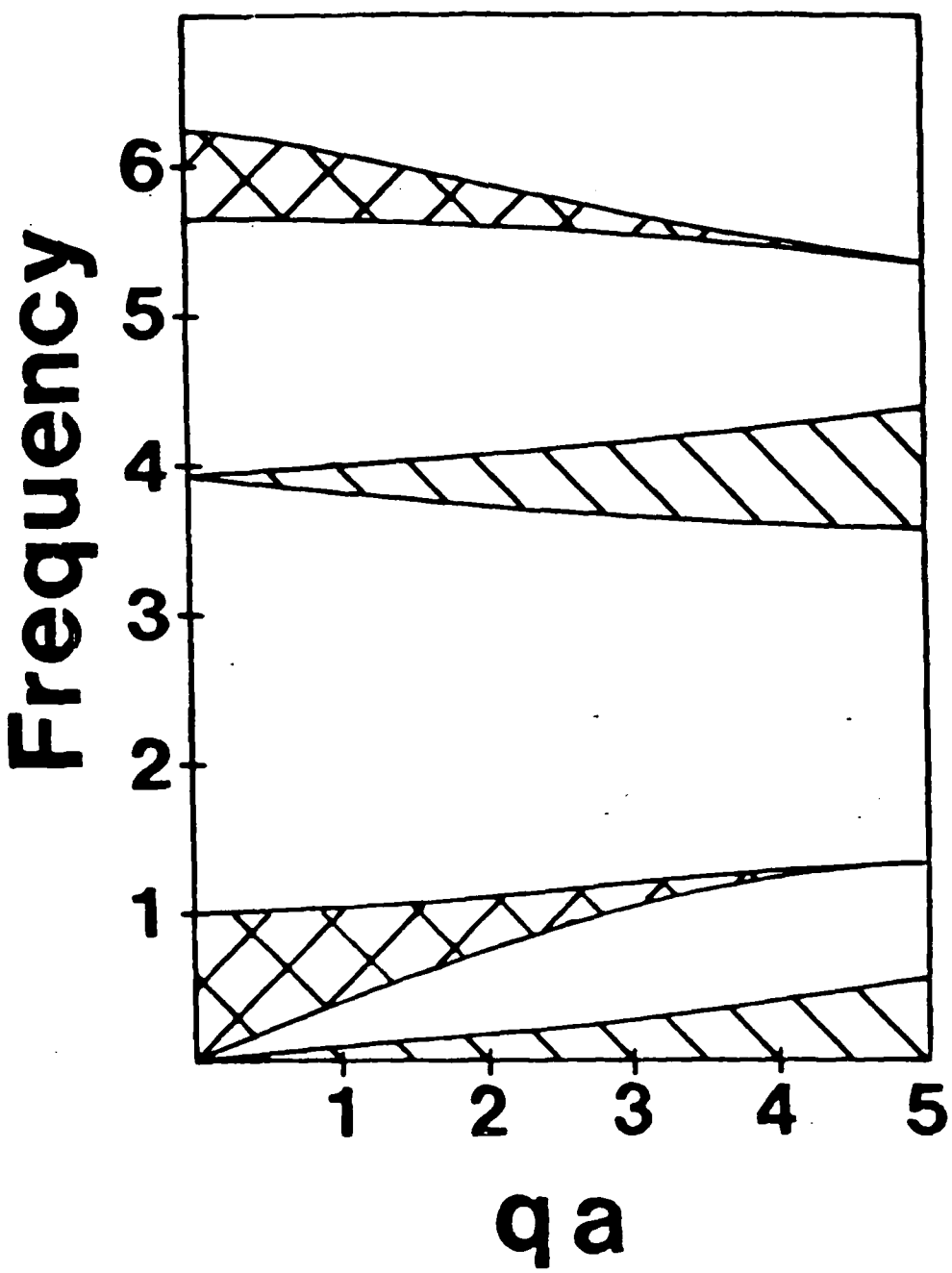
Frequency
6
5
4
3
2
1
1
2
3
4
5
qa

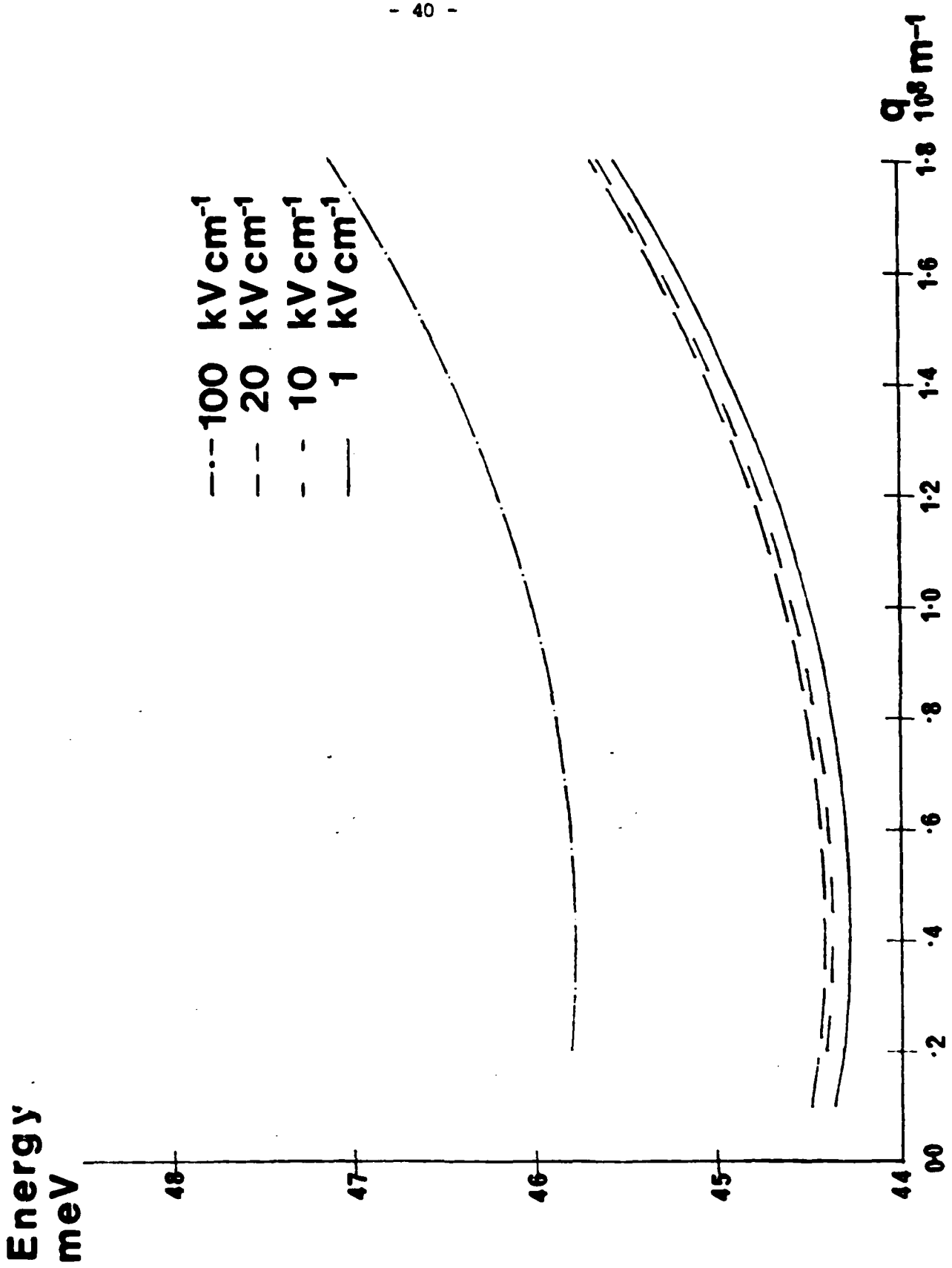
Energy
meV
48
47
46
45
44
0·0
·2
·4
·6
·8
1·0
1·2
1·4
1·6
1·8
q_{10^8} m^{-1}
100 kVcm^{-1}
20 kVcm^{-1}
10 kVcm^{-1}
1 kVcm^{-1}

END

2-87

DTIC